

Neutrino mass hierarchy and electron neutrino oscillation parameters with one hundred thousand reactor events

F. Capozzi,^{1,2} E. Lisi,² and A. Marrone^{1,2}

¹ *Dipartimento Interateneo di Fisica “Michelangelo Merlin,” Via Amendola 173, 70126 Bari, Italy*

² *Istituto Nazionale di Fisica Nucleare, Sezione di Bari, Via Orabona 4, 70126 Bari, Italy*

Proposed medium-baseline reactor neutrino experiments offer unprecedented opportunities to probe, at the same time, the mass-mixing parameters which govern ν_e oscillations both at short wavelength (δm^2 and θ_{12}) and at long wavelength (Δm^2 and θ_{13}), as well as their tiny interference effects related to the mass hierarchy (i.e., the relative sign of Δm^2 and δm^2). In order to take full advantage of these opportunities, precision calculations and refined statistical analyses of event spectra are required. In such a context, we revisit several input ingredients, including: nucleon recoil in inverse beta decay and its impact on energy reconstruction and resolution, hierarchy and matter effects in the oscillation probability, spread of reactor distances, irreducible backgrounds from geoneutrinos and from far reactors, and degeneracies between energy scale and spectrum shape uncertainties. We also introduce a continuous parameter α , which interpolates smoothly between normal hierarchy ($\alpha = +1$) and inverted hierarchy ($\alpha = -1$). The determination of the hierarchy is then transformed from a test of hypothesis to a parameter estimation, with a sensitivity given by the distance of the true case (either $\alpha = +1$ or $\alpha = -1$) from the “undecidable” case ($\alpha = 0$). Numerical experiments are performed for the specific set up envisaged for the JUNO project, assuming a realistic sample of $O(10^5)$ reactor events. We find a typical sensitivity of $\sim 2\sigma$ to the hierarchy in JUNO, which, however, can be challenged by energy scale and spectrum shape systematics, whose possible conspiracy effects are investigated. The prospective accuracy reachable for the other mass-mixing parameters is also discussed.

PACS numbers: 14.60.Pq, 13.15.+g, 28.50.Hw

I. INTRODUCTION

In $\bar{\nu}_e$ disappearance searches with reactor neutrinos, the survival probability $P_{ee} = P(\bar{\nu}_e \rightarrow \bar{\nu}_e)$ is generally not invariant under a swap of the neutrino mass ordering between normal hierarchy (NH) and inverted hierarchy (IH) [1]. The possible discrimination of the hierarchy via high-statistics reactor neutrino experiments at medium baseline (few tens of km) was originally proposed in [2] and is now a very active and promising field of research [3]. The main idea is to probe, at the same time, the mass-mixing parameters which govern ν_e oscillations at short wavelength (δm^2 , θ_{12}) and at long wavelength (Δm^2 , θ_{13}), as well as their tiny interference effects which depend on the mass hierarchy, $\text{sign}(\Delta m^2/\delta m^2)$ [2, 4]. The relatively large value of θ_{13} established in 2012 via $\bar{\nu}_e$ disappearance at short baseline reactors [5–10], in agreement with appearance measurements at long-baseline accelerators [11–13] and with previous indications from global analyses [14, 15], makes the hierarchy-dependent interference effects large enough to be possibly observed in future, dedicated reactor experiments, such as the so-called RENO-50 [16] and JUNO projects [17–19].¹

The literature in this field is rapidly growing. An incomplete list of pre-2012 studies following [2, 4] includes early tentative experimental projects [20], theoretical aspects in comparing disappearance probabilities for NH and IH with floating oscillation parameters [21–23], prospective data analyses with Fourier transform techniques [24–27] also compared with χ^2 analyses [28]. Post-2012 studies have focused on the characterization of more detailed and realistic requirements needed to achieve hierarchy discrimination, such as: detector exposure and energy resolution [29, 30], peak structure resolution [31], optimal baselines [29, 30], multiple reactors effects [17, 32, 33], energy scale uncertainties [17, 28, 34–36], statistical tests of different hierarchy hypotheses [30, 37, 38] and possible synergy [39] with future, independent constraints on Δm^2 [17, 40, 41]; see also [42] for a very recent review and up-to-date results on prospective data fits. All these studies generally find that the hierarchy discrimination should be possible at a significance level of $\gtrsim 2\sigma$, provided that one can achieve unprecedented levels of detector performance and collected

¹ The JUNO (Jiangmen Underground Neutrino Observatory) project [19] was previously called “Daya Bay II” [17, 18]. Within this work, we assume the JUNO project features as reported in [17].

statistics, which will require the control of several systematics at (sub)percent level. Such demanding experimental goals must be matched by accurate theoretical calculations of reactor event spectra and by refined statistical analyses.

In this context, we think it is useful to investigate in more detail some issues related to the precision calculation and the statistical analysis of reactor event spectra, which may provide a useful complement to previous studies in this field. Whenever possible, we shall highlight analytical results of general applicability. Numerical results will instead refer to a specific experimental set-up, namely, the JUNO configuration described in detail in [17], including far-reactor and geoneutrino contributions.

The structure of our work is as follows. In Sec. II we present the basic notation and conventions. In Sec. III and IV we revisit, from an analytical viewpoint, (sub)percent spectral effects related to nucleon recoil and to neutrino oscillations in matter, respectively. We also introduce a useful continuous parameter α , which interpolates smoothly between normal hierarchy ($\alpha = +1$) and inverted hierarchy ($\alpha = -1$). In Sec V we discuss the ingredients of our numerical and statistical analysis of hypothetical samples of $O(10^5)$ reactor events in a JUNO-like experiment. In Sec. VI we present the results of the analysis, and discuss the prospective sensitivity to the hierarchy in terms of the distance between the true case (either $\alpha = +1$ or $\alpha = -1$) and the “undecidable” null case ($\alpha = 0$). The prospective accuracy expected for the relevant mass-mixing parameters is also reported. In Sec. VII we separately discuss several subtle issues raised by the interplay of energy scale and spectrum shape uncertainties. We summarize our work in Sec. VIII.

II. NOTATION

We present below the basic notation used in this work. Explicit definitions are also needed to avoid confusion with similar (but not necessarily equivalent) conventions reported in the literature.

Concerning the neutrino mass-mixing parameters, the squared mass differences and the associated vacuum phases are defined as

$$\Delta m_{ij}^2 = m_i^2 - m_j^2, \quad \Delta_{ij} = \frac{\Delta m_{ij}^2 L}{4E}, \quad (1)$$

where m_i are the neutrino masses, E is the neutrino energy, and L is the baseline, in natural units. As in previous papers [1, 14, 15], we use a specific notation for the “small” and “large” squared mass differences (and phases),

$$\delta m^2 = \Delta m_{21}^2 > 0, \quad \delta = \frac{\delta m^2 L}{4E} > 0, \quad (2)$$

$$\Delta m^2 = \frac{1}{2} |\Delta m_{31}^2 + \Delta m_{32}^2| > 0, \quad \Delta = \frac{\Delta m^2 L}{4E} > 0. \quad (3)$$

Note that, hereafter, δ will represent the vacuum oscillation phase related to δm^2 , and not a possible Dirac phase related to CP violation (δ_{CP}). The two possible hierarchies are distinguished by a discrete parameter α ,

$$\alpha = \begin{cases} +1 & (\text{normal hierarchy}), \\ -1 & (\text{inverted hierarchy}), \end{cases} \quad (4)$$

which will be transformed into a continuous variable in Sec. IV. Trigonometric functions of the mixing angles θ_{ij} (in standard notation [43]) are abbreviated as

$$c_{ij} = \cos \theta_{ij}, \quad s_{ij} = \sin \theta_{ij}. \quad (5)$$

Concerning the inverse beta decay (IBD) process,

$$\bar{\nu}_e + p \rightarrow e^+ + n, \quad (6)$$

the relevant information is contained in the IBD event spectrum S as a function of the observed “visible” energy of the event. The spectrum S is obtained by integrating out the (unobservable) true energies of the incoming neutrino and of the outgoing positron,

$$S(E_{\text{vis}}) = \varepsilon(E_{\text{vis}}) \int_{m_e}^{\infty} dE_e \int_{E_T}^{\infty} dE \left(\sum_i \mathcal{N}_i \Phi_i(E) P_i(E) \right) \frac{d\sigma(E, E_e)}{dE_e} r(E_e + m_e, E_{\text{vis}}), \quad (7)$$

where

$$S(E_{\text{vis}}) = \text{spectrum of events per unit of energy,} \quad (8)$$

$$E = \bar{\nu}_e \text{ energy,} \quad (9)$$

$$E_T = E \text{ threshold for IBD,} \quad (10)$$

$$E_e = \text{true positron energy (total),} \quad (11)$$

$$m_e = \text{positron mass} \quad (12)$$

$$d\sigma(E, E_e)/dE_e = \text{IBD differential cross section,} \quad (13)$$

$$E_e + m_e = \text{true visible energy of the event,} \quad (14)$$

$$E_{\text{vis}} = \text{observed visible energy of the event,} \quad (15)$$

$$r(E_e + m_e, E_{\text{vis}}) = \text{energy resolution function,} \quad (16)$$

$$\varepsilon(E_{\text{vis}}) = \text{detector efficiency,} \quad (17)$$

$$i = \bar{\nu}_e \text{ source index,} \quad (18)$$

$$\Phi_i(E) = \bar{\nu}_e \text{ flux (per unit of energy, area and time),} \quad (19)$$

$$P_i(E) = \bar{\nu}_e \text{ survival probability,} \quad (20)$$

$$\mathcal{N}_i = \text{normalization and conversion factor.} \quad (21)$$

In the above equations, integration over time is implicit: the source fluxes Φ_i or the detector efficiency ε should be understood either as constants or as time averages, unless otherwise stated. Further details on these and related ingredients of the analysis are described in the following sections.

III. RECOIL EFFECTS IN IBD

The kinematics and dynamics of IBD cross section have been thoroughly studied in [44–46]. Here we revisit nucleon recoil effects on reactor spectra, which are not entirely negligible (as it is often assumed) in the context of high-precision experiments. We show that such effects can be included in the calculation of (un)binned reactor neutrino event spectra, through appropriate modifications of the energy resolution function.

A. Positron energy spectrum at fixed neutrino energy E

The IBD kinematical threshold is given by

$$E \geq E_T = [(m_n + m_e)^2 - m_p^2] / 2m_p = 1.806 \text{ MeV} , \quad (22)$$

where m_p and m_n are the proton and neutron masses, respectively. In the popular “recoilless” approximation, the positron energy E_e is directly linked to the neutrino energy E via $E - E_e \simeq \Delta_{np}$ (where $\Delta_{np} = m_n - m_p = 1.293 \text{ MeV}$). However, since a small fraction of energy [of $O(E/m_p)$] is carried by the recoiling nucleon, this estimate provides only an approximate upper bound to E_e . More precisely, E_e falls within a well-defined kinematical range,

$$E_e \in [E_1, E_2] , \quad (23)$$

where explicit expressions for $E_{1,2}$ can be found, e.g., in [46]. For E largely above threshold, the boundaries of the neutrino-positron energy difference $E - E_e$ are approximately given by

$$E - E_2 \simeq \Delta_{np} , \quad (24)$$

$$E - E_1 \simeq \Delta_{np} + 2(E - \Delta_{np})E/m_p . \quad (25)$$

Figure 1 reports the exact boundaries (with no approximation) as a function of E . From this figure and from the above expressions it appears that, in the high-energy tail of the reactor spectrum ($E \simeq 6\text{--}8 \text{ MeV}$), recoil corrections can reach the percent level, comparable to the prospective energy scale accuracy and resolution width [17, 34] in the same range. We emphasize that the correction to the recoilless approximation is twofold: at any given E , the typical E_e energy is displaced at $O(E/m_p)$ and it also acquires a spread of $O(E/m_p)$. Both effects can be taken into account as follows.

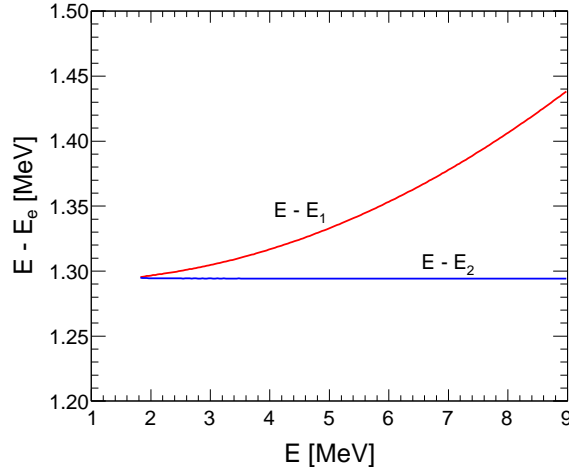


FIG. 1: Inverse beta decay: Range of the difference between the $\bar{\nu}_e$ energy (E) and the e^+ energy (E_e), as a function of E . The extrema are indicated as $E - E_1$ and $E - E_2$. See the text for details.

Within the narrow range $[E_1, E_2]$, the IBD dynamics governs the spectral distribution of E_e , i.e., the normalized differential cross section $\sigma^{-1}d\sigma/dE_e$. Figure 2 shows this distribution in terms of deviations of E_e from its mid-value, $\Delta E_e = E_e - (E_1 + E_2)/2$, for selected values of the neutrino energy E . For definiteness, we have used the cross section as taken from [46]. At small energies, the distributions in Fig. 2 approach the “Dirac deltas” expected in the recoilless approximation, while at high energies there is a noticeable spread. For our purposes (see the next subsection) each distribution can be approximated by a “top hat” function for $E_e \in [E_1, E_2]$:

$$\frac{1}{\sigma(E)} \frac{d\sigma(E, E_e)}{dE_e} \simeq \frac{1}{E_2 - E_1}, \quad (26)$$

where $\sigma(E) = \int dE_e (d\sigma/dE_e)$. We have verified that further corrections related to the slight slopes in Fig. 2 are completely negligible in the calculation of observable event spectra.

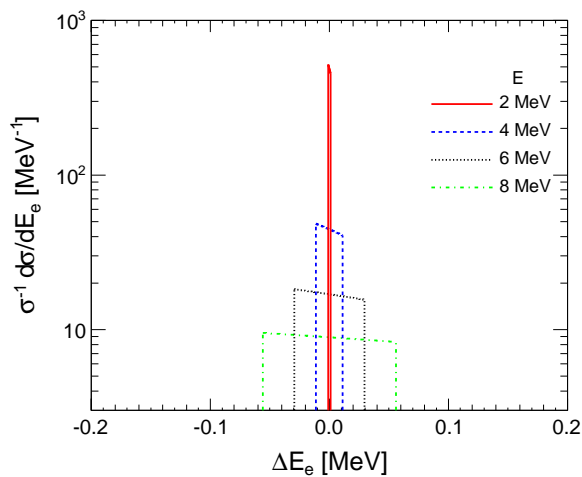


FIG. 2: Inverse beta decay: shape of the e^+ energy spectrum for representative values of the $\bar{\nu}_e$ energy E . The spectra are aligned to their median value for graphical convenience.

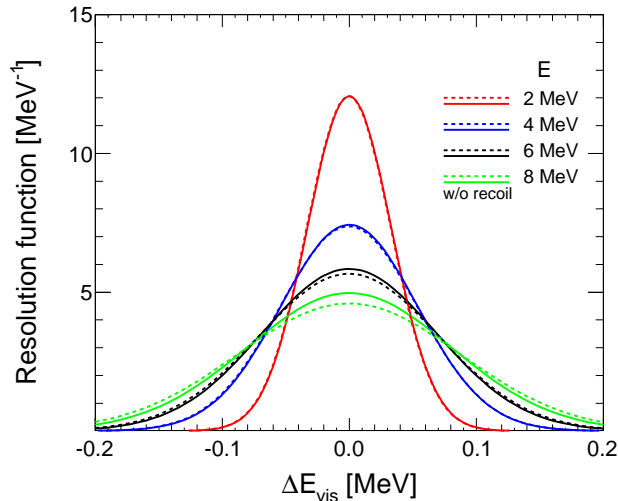


FIG. 3: Energy resolution function without (solid) and with (dashed) the inclusion of nucleon recoil effects, for the same representative values of the neutrino energy E as in Fig. 2. The functions are aligned to their median value for graphical convenience.

B. Recoil effects in unbinned spectra

For any detected IBD event, the observed visible energy E_{vis} may differ from the true visible energy $E_e + m_e$, due to intrinsic fluctuations in the collected photon statistics and other possible uncertainties. We assume a gaussian form for the corresponding energy resolution function r ,

$$r(E_e + m_e, E_{\text{vis}}) = \frac{1}{\sigma_e(E_e)\sqrt{2\pi}} \exp\left[-\frac{1}{2}\left(\frac{E_{\text{vis}} - E_e - m_e}{\sigma_e(E_e)}\right)^2\right], \quad (27)$$

with a prospective width [17]

$$\frac{\sigma_e(E_e)}{E_e + m_e} = \frac{3 \times 10^{-2}}{\sqrt{(E_e + m_e)/\text{MeV}}} \quad (28)$$

which decreases from $\sim 3\%$ at $E \sim 2$ MeV to $\sim 1\%$ at $E \sim 8$ MeV.

Various assumptions and empirical parametrizations for the width σ_e have been studied elsewhere (see, e.g., [17, 29–31, 34, 42] for recent examples), showing that it is imperative to have σ_e as small as possible, i.e., close to the ideal limit of full light collection. The empirical form of σ_e in a real detector is actually determined by a combination of calibration experiments and light-yield MonteCarlo simulations, which fix at the same time the energy scale and the energy resolution, as well as their correlated uncertainties [47]. In this work we do not deal with these subtle experimental aspects, and simply assume σ_e as in the above equation; we instead focus on the inclusion of recoil effects of $O(E/m_p)$ which, as noted, can be as large as $O(\sigma_e/E)$ for $E \simeq 8$ MeV.

In the approximation of Eq. (26) and for a gaussian resolution function as in Eq. (27), the inner integral of the continuous (unbinned) spectrum S in Eq. (7) can be performed analytically, yielding:

$$S(E_{\text{vis}}) = \varepsilon(E_{\text{vis}}) \int_{E_T}^{\infty} dE \left(\sum_i \mathcal{N}_i \Phi_i(E) P_i(E) \right) \frac{\sigma(E)}{E_2 - E_1} \int_{E_1}^{E_2} dE_e r(E_e + m_e, E_{\text{vis}}) \quad (29)$$

$$= \varepsilon(E_{\text{vis}}) \int_{E_T}^{\infty} dE \left(\sum_i \mathcal{N}_i \Phi_i(E) P_i(E) \right) \sigma(E) R(E, E_{\text{vis}}) \quad (30)$$

where R is the recoil-corrected energy resolution function,

$$R(E, E_{\text{vis}}) = \frac{1}{2(E_2 - E_1)} \left[\text{erf}\left(\frac{E_2 + m_e - E_{\text{vis}}}{\sqrt{2}\sigma_e}\right) - \text{erf}\left(\frac{E_1 + m_e - E_{\text{vis}}}{\sqrt{2}\sigma_e}\right) \right], \quad (31)$$

with $\text{erf}(x)$ defined as [48]

$$\text{erf}(x) = \frac{2}{\sqrt{\pi}} \int_0^x dt e^{-t^2} . \quad (32)$$

The function R in Eq. (31) reduces to the function r in Eq. (27) in the recoilless limit.

Figure 3 compares the energy resolution functions with recoil (R) and without recoil (r), as solid and dotted lines, respectively, for different neutrino energies E . All functions are aligned to their average visible energy, which is also the origin of the x -axis scale ΔE_{vis} . The alignment removes one of the recoil effects [the relative displacement of centroids at $O(E/m_p)$] in order to emphasize the other effect, namely, the widening of the energy resolution tails.

Summarizing, nucleon recoil effects can be implemented in the unbinned spectrum S by using the modified energy resolution function R in Eq. (31), instead of the usual function r in Eq. (27). Similar results hold for a binned spectrum as described below.

C. Recoil effects in binned spectra

Although we shall focus on unbinned spectral analyses in Sec. V C, for completeness we also discuss recoil effects in binned spectra, in the realistic case where the efficiency function $\varepsilon(E_{\text{vis}})$ is smooth enough to be nearly constant in each bin. Let us consider a spectrum S divided into bins, the i -th one covering a range $E_{\text{vis}} \in [E'_i, E''_i]$ and containing a number of events given by

$$N_i = \int_{E'_i}^{E''_i} dE_{\text{vis}} S(E_{\text{vis}}) . \quad (33)$$

Since S is a double integral [see Eq. (7)], the calculation of N_i involves in general a triple integral, $\int dE_{\text{vis}} \int dE_e \int dE$. A useful reduction is possible if the efficiency function $\varepsilon(E_{\text{vis}})$ can be taken as approximately constant in each bin range, namely, $\varepsilon(E_{\text{vis}}) \simeq \varepsilon_i$ for $E_{\text{vis}} \in [E'_i, E''_i]$. In this case, the integration ordering can be swapped into $\int dE \int dE_e \int dE_{\text{vis}}$, where the two inner integrals are analytical. A similar reduction was used in [49] in another context. The final result is:

$$N_i = \varepsilon_i \int_{E_T}^{\infty} dE \left(\sum_i \mathcal{N}_i \Phi_i(E) P_i(E) \right) \sigma(E) W_i(E) , \quad (34)$$

where the function $W_i(E)$ is given by

$$W_i(E) = \frac{\sqrt{2}\sigma_e}{2(E_2 - E_1)} [g(E''_i - E_1) - g(E''_i - E_2) - g(E'_i - E_1) + g(E'_i - E_2)] , \quad (35)$$

and

$$g(x) = \frac{x - m_e}{\sqrt{2}\sigma_e} \text{erf} \left(\frac{x - m_e}{\sqrt{2}\sigma_e} \right) + \frac{1}{\sqrt{\pi}} e^{-\left(\frac{x - m_e}{\sqrt{2}\sigma_e}\right)^2} . \quad (36)$$

In the above formulae, tiny variations of σ_e for $E_e \in [E_1, E_2]$ have been neglected [e.g., the value of σ_e can be taken at $E_e = (E_1 + E_2)/2$]. In the limit of no recoil and perfect resolution ($\sigma_e \rightarrow 0$), W_i reduces to a top-hat function of width $E''_i - E'_i$; finite resolution and recoil effects smear out the top-hat shape. In conclusion, with or without binning, recoil effects on the event spectrum can be included in terms of a single integral over the neutrino energy E with appropriate kernels, according to Eqs. (30) and (34).

IV. OSCILLATION PROBABILITY

In this Section we discuss in detail the reactor neutrino survival probability P_{ee} . We cast P_{ee} in a closed analytical form, including matter and multiple reactor effects [see Eq. (58) below]. This form allows to make the discrete parameter α in Eq. (4) continuous, so as to interpolate smoothly between NH ($\alpha = +1$) and IH ($\alpha = -1$). In this way one can cover the null case of “undecidable” hierarchy ($\alpha = 0$) in the subsequent statistical analysis.

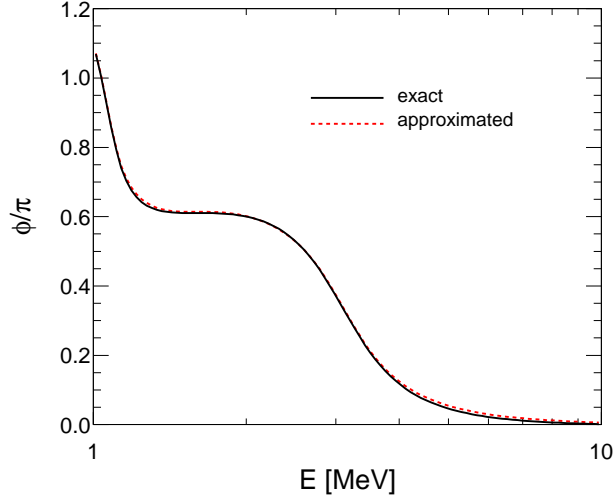


FIG. 4: Comparison of exact and approximate values (in units of π) of the phase contribution φ embedding hierarchy effects, as a function of neutrino energy E , for $s_{12}^2 = 0.307$, $\delta m^2 = 7.54 \times 10^{-5} \text{ eV}^2$, and $L = 52.5 \text{ km}$. See the text for details.

A. Oscillation probability in vacuum

Using the notation in Sec. II, the 3ν vacuum survival probability $P(\bar{\nu}_e \rightarrow \bar{\nu}_e)$ can be written in the form

$$P_{\text{vac}}^{3\nu} = 1 - 4c_{13}^4 s_{12}^2 c_{12}^2 \sin^2 \delta - 4s_{13}^2 c_{13}^2 c_{12}^2 \sin^2(\alpha\Delta + \delta/2) - 4s_{13}^2 c_{13}^2 s_{12}^2 \sin^2(-\alpha\Delta + \delta/2). \quad (37)$$

As observed in [1], the above expression is not invariant under a change of hierarchy ($\alpha \rightarrow -\alpha$), except for the case $c_{12}^2 = s_{12}^2$ which is experimentally excluded.

It is tempting to separate α -odd terms in the oscillation *amplitudes*. However, these terms carry a spurious dependence on the conventional squared mass parameter which is kept fixed while its sign is flipped. For instance, α -odd terms at fixed Δm^2 in Eq. (37) are proportional to $\sin \delta$,

$$P_{\text{odd}}^{3\nu} = 2\alpha s_{13}^2 c_{13}^2 (s_{12}^2 - c_{12}^2) \sin(2\Delta) \sin \delta, \quad (38)$$

while α -odd terms at fixed Δm_{31}^2 [30] or fixed Δm_{32}^2 [50] are proportional to $\sin 2\delta$. Convention-independent effects should not impose that the largest squared mass difference (be it Δm_{31}^2 , or Δm_{32}^2 , or a combination such as Δm^2) is the same in NH and IH. It is thus incorrect to claim, on this basis, that $\sin 2\delta = 1$ is an optimal condition to observe hierarchy effects in reactor experiments [50].

In order to circumvent this drawback, one may separate α -odd terms in the oscillation *phase* without fixing the squared mass parameter, as proposed in [22, 23] and revisited in [31, 34]. In particular, the probability $P_{\text{vac}}^{3\nu}$ in Eq. (37) can be exactly rewritten as [23]:

$$P_{\text{vac}}^{3\nu} = c_{13}^4 P_{\text{vac}}^{2\nu} + s_{13}^4 + 2s_{13}^2 c_{13}^2 \sqrt{P_{\text{vac}}^{2\nu}} \cos(2\Delta_{ee} + \alpha\varphi), \quad (39)$$

in terms of the 2ν limit

$$P_{\text{vac}}^{2\nu} = \lim_{\theta_{13} \rightarrow 0} P_{\text{vac}}^{3\nu} = 1 - 4s_{12}^2 c_{12}^2 \sin^2 \delta, \quad (40)$$

and of an effective squared mass parameter [21–23],

$$\Delta m_{ee}^2 = \Delta m^2 + \frac{\alpha}{2}(c_{12}^2 - s_{12}^2)\delta m^2, \quad (41)$$

with

$$\Delta_{ee} = \frac{\Delta m_{ee}^2 L}{4E} = \Delta + \frac{\alpha}{2}(c_{12}^2 - s_{12}^2)\delta, \quad (42)$$

while the phase φ in Eq. (39) is parametrically defined as [23, 39]

$$\cos \varphi = \frac{c_{12}^2 \cos(2s_{12}^2 \delta) + s_{12}^2 \cos(2c_{12}^2 \delta)}{\sqrt{P_{\text{vac}}^{2\nu}}}, \quad (43)$$

$$\sin \varphi = \frac{c_{12}^2 \sin(2s_{12}^2 \delta) - s_{12}^2 \sin(2c_{12}^2 \delta)}{\sqrt{P_{\text{vac}}^{2\nu}}}. \quad (44)$$

Equation (39) also allows a clear separation between “fast” (Δ_{ee} -driven) oscillations and “slow” (δ -driven) modulations in $P_{\text{vac}}^{2\nu}$ and φ .

Expressing φ via an arctan function [from the ratio of Eqs. (44) and (43)] is not particularly convenient as it leads to a quadrant ambiguity. We have found a useful empirical approximation to φ in closed form,

$$\varphi \simeq 2s_{12}^2 \delta \left(1 - \frac{\sin \delta}{2\delta \sqrt{P_{\text{vac}}^{2\nu}}} \right), \quad (45)$$

which will be used hereafter. Figure 4 shows a comparison of exact and approximate values of φ as a function of neutrino energy E , calculated for reference values $s_{12}^2 = 0.307$, $\delta m^2 = 7.54 \times 10^{-5} \text{ eV}^2$, and $L = 52.5 \text{ km}$. The numerical differences are negligible for any practical purpose. Similar results (not shown) hold for s_{12}^2 and δm^2 taken in their $\pm 3\sigma$ phenomenological range [15]. In addition, the approximate expression for φ [Eq. (45)] shares two analytical properties of the exact parametric definition of φ [Eqs. (43) and (44)], namely: it periodically increases with δ as $\varphi(\delta + \pi) = \varphi(\delta) + 2\pi s_{12}^2$ [23], and it starts with a cubic term (δ^3) in a power expansion [31].

As it was emphasized in [23] and later in [31, 34], the hierarchy dependence of $P_{\text{vac}}^{3\nu}$ is physically manifest in the odd term $\pm\varphi$, which induces either an observable advancement ($+\varphi$) or a retardation ($-\varphi$) of the oscillation phase, with a peculiar energy dependence *not* proportional to L/E (see Fig. 4). Conversely, hierarchy-odd effect which are proportional to L/E [as in Eq. (42)] are immaterial, as far as they can be absorbed into a redefinition of Δm^2 within experimental uncertainties. Determining the hierarchy with reactor experiments thus amounts to finding evidence for an extra, non- L/E oscillation phase with definite sign (either $+\varphi$ or $-\varphi$), for unconstrained values of Δm_{ee}^2 . This requirement places the focus of the measurement on the low-energy part of the spectrum where φ is large, while the high-energy part acts as a calibration.

B. Multiple reactor cores

In the presence of $n = 1, \dots, N$ reactor cores (placed at slightly different distances L_n and contributing with different fluxes Φ_n), damping effects arise on the fast oscillating terms, while being negligible on the slow ones [17, 33]. Such effects can be taken into account analytically as follows.

Let us define the flux weights w_n , the flux-weighted baseline L , and the fractional baseline differences λ_n as

$$w_n = \frac{\Phi_n}{\sum_n \Phi_n}, \quad (46)$$

$$L = \sum_n w_n L_n, \quad (47)$$

$$\lambda_n = \frac{L_n - L}{L}, \quad (48)$$

where $\sum_n w_n = 1$ and $\sum_n \lambda_n = 0$. The fast oscillating term in $P_{\text{vac}}^{3\nu}$ is obtained by summing up the weighted contributions from different cores,

$$P_{\text{vac}}^{3\nu} \simeq c_{13}^4 P_{\text{vac}}^{2\nu} + s_{13}^4 + 2s_{13}^2 c_{13}^2 \sqrt{P_{\text{vac}}^{2\nu}} \sum_n w_n \cos\left(\frac{\Delta m_{ee}^2 L_n}{2E} + \alpha\varphi\right), \quad (49)$$

and by reducing it via the trigonometric identity

$$\sum_n w_n \cos(x + \xi_n) = w \cos(x + \xi), \quad (50)$$

where

$$w^2 = \sum_{n,m} w_n w_m \cos(\xi_n - \xi_m), \quad (51)$$

$$\tan \xi = \frac{\sum_n w_n \sin \xi_n}{\sum_n w_n \cos \xi_n}. \quad (52)$$

In our case, $x = (\Delta m_{ee}^2 L/2E) + \alpha\varphi$ and $\xi_n = \Delta m_{ee}^2 L\lambda_n/2E$. By keeping the first nontrivial terms in a ξ and ξ_n power expansion, the final result can be cast in the form

$$P_{\text{vac}}^{3\nu} \simeq c_{13}^4 P_{\text{vac}}^{2\nu} + s_{13}^4 + 2s_{13}^2 c_{13}^2 \sqrt{P_{\text{vac}}^{2\nu}} w \cos(2\Delta_{ee} + \alpha\varphi), \quad (53)$$

where the damping factor w reads

$$w \simeq 1 - 2(\Delta_{ee})^2 \sum_n w_n \lambda_n^2. \quad (54)$$

Let us consider the specific JUNO setting, characterized by $N = 10$ reactor cores (6 being located at Yangjiang and 4 at Taishan) with average power P_n [17]. Assuming fluxes $\Phi_n \propto P_n/L_n^2$, we obtain a flux-weighted distance $L = 52.474$ km and a damping coefficient $\sum_n w_n \lambda_n^2 = 2.16 \times 10^{-5}$. In this case, the amplitude of the hierarchy-sensitive cosine term in Eq. (53) is reduced by as much as 28% at low energy ($E \simeq 2$ MeV).

Finally, we remark that damping effects may acquire a slight time dependence via reactor power variations, $P_n = P_n(t)$. This dependence may be effectively embedded in time-dependent weights $w_n = w_n(t)$, baseline $L = L(t)$ and damping factor $w = w(t)$. For the sake of simplicity, we shall only consider stationary conditions (constant L and w) hereafter.

C. Oscillation probability in matter

At medium baselines $L \sim O(50)$ km, reactor $\bar{\nu}_e$ mostly propagate within the upper part of the Earth's crust. For a nearly constant electron density N_e , the ratio of matter to vacuum terms in the propagation hamiltonian reads [55]

$$\mu_{ij} = \frac{2\sqrt{2}G_F N_e E}{\Delta m_{ij}^2} = 1.526 \times 10^{-7} \left(\frac{N_e}{\text{mol/cm}^3} \right) \left(\frac{E}{\text{MeV}} \right) \left(\frac{\text{eV}^2}{\Delta m_{ij}^2} \right). \quad (55)$$

Assuming a typical crust density $N_e \simeq 1.3$ mol/cm³, the only non-negligible ratio is $\mu_{12} \sim O(10^{-2})$. Correspondingly, the (ν_1, ν_2) mass-mixing parameters in matter $(\delta\tilde{m}^2, \tilde{\theta}_{12})$ [55] read, at first order in μ_{12} and for $\bar{\nu}_e$ oscillations,

$$\sin 2\tilde{\theta}_{12} \simeq \sin 2\theta_{12}(1 - \mu_{12} \cos 2\theta_{12}), \quad (56)$$

$$\delta\tilde{m}^2 \simeq \delta m^2(1 + \mu_{12} \cos 2\theta_{12}). \quad (57)$$

Note that, for $E \sim 8$ MeV, the fractional matter correction to mass-mixing parameters is $\sim 8 \times 10^{-3}$, which is definitely not negligible as compared with the prospective fit accuracy on the same parameters (see below).

We implement matter effects via the replacement $(\delta m^2, \theta_{12}) \rightarrow (\delta\tilde{m}^2, \tilde{\theta}_{12})$ from Eqs. (56,57) into $P_{\text{vac}}^{2\nu}$, obtaining as a final result

$$P_{\text{mat}}^{3\nu} \simeq c_{13}^4 P_{\text{mat}}^{2\nu} + s_{13}^4 + 2s_{13}^2 c_{13}^2 \sqrt{P_{\text{mat}}^{2\nu}} w \cos(2\Delta_{ee} + \alpha\varphi), \quad (58)$$

where

$$P_{\text{mat}}^{2\nu} = 1 - 4\tilde{s}_{12}^2 \tilde{c}_{12}^2 \sin^2 \tilde{\delta}. \quad (59)$$

These two equations provide our ‘‘master formula’’ for the oscillation probability in either NH ($\alpha = +1$) or IH ($\alpha = -1$), including matter effects in the crust and damping effects of multiple reactor cores.

A final remark is in order. We have omitted the replacement $(\delta m^2, \theta_{12}) \rightarrow (\delta\tilde{m}^2, \tilde{\theta}_{12})$ into φ , since it leads to insignificant numerical variations of $P_{\text{mat}}^{3\nu}$. We have also compared the above $P_{\text{mat}}^{3\nu}$ with the exact probability derived from numerical flavor evolution in matter of $\bar{\nu}_e$'s from each single reactor source,

$$P_{\text{exact}}^{3\nu} = \sum_n w_n P_{\text{exact}}^{3\nu}(L_n, E, N_e, \delta m^2, \Delta m_{ee}^2, \theta_{12}, \theta_{13}, \alpha), \quad (60)$$

for $\alpha = \pm 1$, obtaining permill-level differences ($|P_{\text{mat}}^{3\nu} - P_{\text{exact}}^{3\nu}| < 2 \times 10^{-3}$ for $E \geq E_T$) which can be safely neglected in the data analysis. In conclusion, Eq. (58) is a very good approximation to the exact oscillation probability.

D. Continuous “interpolation” between the two hierarchies

The analytical form of P_{ee} in Eq. (58) isolates hierarchy effects via an extra, non- L/E contribution $\pm\varphi$ to the “fast” L/E oscillation phase $2\Delta_{ee}$; then, the sign of the extra phase (i.e., the occurrence of either an advancement or a retardation of phase) can tell the hierarchy [23, 31, 34].

In realistic situations, it may occur that an experiment finds no evidence for an extra phase, or some evidence for it but with the wrong sign, or even with a wrong (too large or too small) amplitude. We propose to cover all these possible outcomes by generalizing the discrete parameter $\alpha = \pm 1$ in Eqs. (4) and (58) as a formally continuous parameter,

$$\alpha = \pm 1 \rightarrow \alpha = \text{free parameter} , \quad (61)$$

whose value should be constrained by a fit to prospective or real data. Evidence for $\alpha \neq 0$ will then translate into evidence for hierarchy effects, with NH or IH being signaled by $\text{sign}(\alpha)$. Viceversa, the hierarchy discrimination will be compromised, if the data favor either the “null” case $\alpha \simeq 0$, or implausible cases with $|\alpha| > 1$.

This phenomenological approach makes the data analysis easier, since α is formally treated as any other free parameter in the fit; moreover, it offers an alternative viewpoint to some subtle statistical issues recently highlighted in [30, 51, 52]. In particular, it appears that the traditional $\Delta\chi^2$ distance between the “true” and “wrong” hierarchy cases, if naively interpreted, may overestimate the real sensitivity to the hierarchy for at least two reasons: (1) $\Delta\chi^2$ is an appropriate statistical measure for (continuous) parameter estimation tests, but not necessarily for (discrete) hypotheses tests; (2) the hierarchy discrimination is already compromised in cases which are half-way between the “true” and “wrong” expectations. Various statistical methods and measures have been introduced in [25, 26, 30, 51, 52] to quantify more properly the hierarchy sensitivity. Our approach offers an alternative perspective by (1) introducing a continuous parameter α which allows usual χ^2 analyses, and (2) comparing the cases $\alpha = \pm 1$ with the null case $\alpha = 0$ in order to estimate the hierarchy sensitivity. See Sec. VI for related comments.

E. Oscillation probability for geoneutrinos and far reactors

In general, medium-baseline reactor experiments designed to probe the hierarchy at $L \sim O(50)$ km suffer from irreducible backgrounds from farther reactors at $L \gg 50$ km [17, 31] (insensitive to Δm^2) and from geoneutrinos [27] (insensitive to both Δm^2 and δm^2). For the “far” and “geo” background components we shall take the oscillation probability as

$$P_{\text{far}}^{3\nu} \simeq c_{13}^4 P_{\text{mat}}^{2\nu} + s_{13}^4 , \quad (62)$$

with $P_{\text{mat}}^{2\nu}$ as in Eq. (59), and

$$P_{\text{geo}}^{3\nu} \simeq c_{13}^4 (1 - 2s_{12}^2 c_{12}^2) + s_{13}^4 , \quad (63)$$

respectively.

We remark that the geoneutrino background may acquire a slight δm^2 dependence through non-averaged oscillation effects in the local crust. These effects, not considered herein, may be estimated or at least constrained by constructing detailed geological models for the local distribution of Th and U geoneutrino sources [53].

V. INGREDIENTS OF THE NUMERICAL AND STATISTICAL ANALYSIS

In the previous Sections I and II we have discussed features of the differential cross section and of the oscillation probabilities, which may be useful for generic medium-baseline reactor experiments. In this section we describe further ingredients which refer to the specific JUNO experimental setting described in [17] and to other choices made in our numerical and statistical analysis.

A. Priors on oscillation parameters

At present, global neutrino data analyses show no significant indication in favor of either normal or inverted hierarchy. We thus conflate the (slightly different) current results for normal and inverted hierarchy as taken from

[15], and assume the following α -independent priors for the relevant oscillation parameters in Eq. (58),

$$\delta m^2/eV^2 = (7.54 \pm 0.24) \times 10^{-5}, \quad (64)$$

$$\Delta m_{ee}^2/eV^2 = (2.43 \pm 0.07) \times 10^{-3}, \quad (65)$$

$$s_{12}^2 = 0.307 \pm 0.017, \quad (66)$$

$$s_{13}^2 = 0.0242 \pm 0.0025, \quad (67)$$

with errors at $\pm 1\sigma$.

B. Fluxes and normalization

In this section we fix the fluxes and normalization factors in the integrand of Eq. (7), namely,

$$\mathcal{N}_{\text{MB}}\Phi_{\text{MB}}P_{\text{mat}}^{3\nu} + \mathcal{N}_{\text{far}}\Phi_{\text{far}}P_{\text{far}}^{3\nu} + \mathcal{N}_{\text{geo}}\Phi_{\text{geo}}P_{\text{geo}}^{3\nu} \quad (68)$$

where, in the context of JUNO, the three terms refer to the contributions from the 10 medium-baseline reactors (MB) [17], the two dominant far-reactor complexes (far) [17], and geoneutrinos (geo) [54], respectively.

The reactor fluxes depend, in general, on the (time-dependent) relative U and Pu fuel components. For our prospective data analysis, we assume typical average values from Fig. 21 in [6],

$${}^{235}\text{U} : {}^{239}\text{Pu} : {}^{238}\text{U} : {}^{241}\text{Pu} \simeq 0.60 : 0.27 : 0.07 : 0.06, \quad (69)$$

for both medium-baseline and far reactors. The corresponding fluxes are taken from [56].

Concerning the reactor event normalization, from the information reported in [6] we derive the following rough estimate for the number of unoscillated events, expected for a detector of mass M at distance L from a reactor complex of thermal power P in typical conditions at Daya Bay (including detection efficiencies and reactor duty cycles):

$$\frac{\text{unoscillated events}}{\text{year}} \simeq 2.65 \times 10^5 \left(\frac{M}{\text{kT}}\right) \left(\frac{P}{\text{GW}}\right) \left(\frac{\text{km}}{L}\right)^2. \quad (70)$$

For our numerical analysis of JUNO, we assume $M = 20$ kT and $P = 35.8$ GW from [17], $L = 52.474$ km from Sec IV D, and an exposure of 5 years, yielding a total of 3.4×10^5 events expected for no oscillations; these numbers fix the normalization of the term $\mathcal{N}_{\text{MB}}\Phi_{\text{MB}}$ after energy integration. Oscillations typically reduce the expectations to $\sim 10^5$ events for oscillation parameters as in Sec. V A, hence the title of this work. Such an oscillated rate corresponds to ~ 55 oscillated events per day in typical conditions.²

By repeating the previous exercise for the two far reactors with power $P = 17.4$ GW at $L = 215$ km and 265 km [17], we obtain 10^4 and 6.5×10^3 unoscillated events in five years, respectively. These estimates fix the normalizations of the two far-reactor subterms in $\mathcal{N}_{\text{far}}\Phi_{\text{far}}$.

Concerning the normalization of geoneutrino events, we assume from [54] the following unoscillated flux estimates near the Daya Bay site (central values): $\Phi(\text{U}) = 4.04 \times 10^6/\text{cm}^2/\text{s}$ and $\Phi(\text{Th}) = 3.72 \times 10^6/\text{cm}^2/\text{s}$, which correspond to unoscillated event rates $R(\text{U}) = 51.7$ TNU and $R(\text{Th}) = 15.0$ TNU, where one terrestrial neutrino unit (TNU) corresponds to 10^{-32} events per target proton per year [57]. Assuming a liquid scintillator detector of 20 kT mass and proton fraction $\sim 11\%$, operating for five years with typical low-energy efficiency $\varepsilon \simeq 0.8$, we estimate an effective geo-neutrino exposure of $\sim 5.2 \times 10^{33}$ in units of protons \times years, which implies $\sim 2.7 \times 10^3$ (U) and $\sim 0.8 \times 10^3$ (Th) unoscillated events, fixing the geoneutrino normalization in our analysis. Concerning the geoneutrino fluxes, we use the same spectral shape as in [53].

Notice that, in the above estimates, typical efficiency factors are already embedded in the normalization factors \mathcal{N} . Therefore, we take $\varepsilon(E_{\text{vis}}) = 1$ in Eq. (7). With all the ingredients described so far, the absolute event spectrum can be calculated for any value of the continuous parameters $(\delta m^2, \Delta m_{ee}^2, \theta_{12}, \theta_{13}, \alpha)$.³

² Our estimate seems more optimistic than the rate of ~ 40 events/day quoted in [19]. We are unable to trace the source(s) of this difference which, if confirmed, could be compensated by rescaling our assumed lifetime from 5 to 6.8 years in order to collect the same event statistics.

³ In this study we have ignored further oscillation-independent backgrounds, see [42] for a recent evaluation in the context of JUNO.

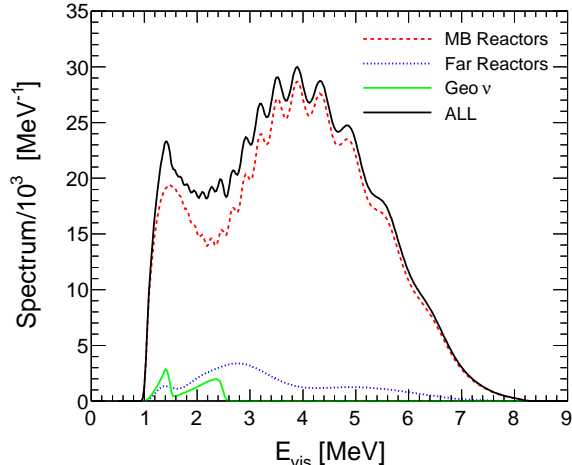


FIG. 5: Absolute energy spectrum of events expected in JUNO for normal hierarchy ($\alpha = +1$) and assuming the central values of the oscillation parameters defined in the text. The breakdown of the total spectrum in its three components (medium baseline reactors, far reactors, geoneutrinos) is also shown

Figure 5 shows the total absolute spectrum of oscillated events and its breakdown into three main components (medium-baseline reactors, far reactors, and geoneutrinos), in terms of the measured visible energy E_{vis} . The calculation refers to normal hierarchy ($\alpha = +1$) and to the central values in Sec. V A. Although the far-reactor component is small, its modulation over the whole energy spectrum affects the determination of the $(\delta m^2, \theta_{12})$ parameters which govern the “slow” oscillations. In addition, the small geoneutrino component adds some “noise” at low energy, where most of the hierarchy information is confined via the phase φ . These effects will be discussed quantitatively in Sec. VI.

For the sake of completeness, Fig. 6 compares the total absolute spectra of oscillated events in the two cases of normal hierarchy ($\alpha = +1$) and inverted hierarchy ($\alpha = -1$). In this figure we have used the same oscillation parameters as in Fig. 5 for both hierarchies, hence the NH and IH spectra merge at high energy where $\varphi \rightarrow 0$. The low-energy differences between the two spectra are generally very small, and may become even smaller with floating mass-mixing parameters, making a detailed statistical analysis mandatory.

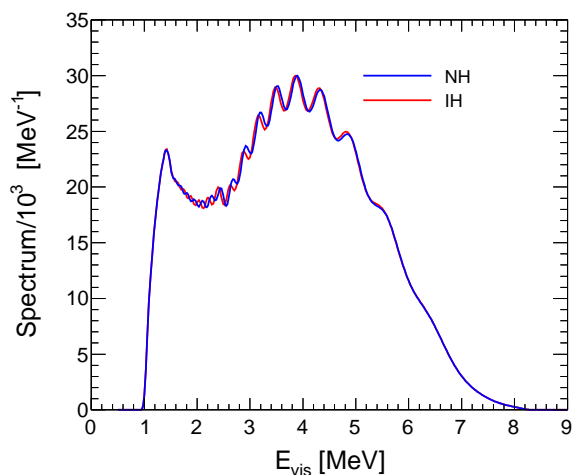


FIG. 6: Comparison of absolute energy spectra of events expected in JUNO for normal hierarchy ($\alpha = +1$) and inverted hierarchy ($\alpha = -1$), assuming in both cases the same oscillation parameters as in Fig. 5.

C. χ^2 function

We assume that the “true” spectrum $S^*(E_{\text{vis}})$ is the one calculated for the central values of the oscillation parameters in Sec. V A and for either normal hierarchy ($\alpha = +1$) or inverted hierarchy ($\alpha = -1$). The “true” spectrum S^* is then compared with a family of spectra $S(E_{\text{vis}})$ obtained by varying the continuous parameters (δm^2 , Δm_{ee}^2 , θ_{12} , θ_{13} , α), in terms of a χ^2 function which contains statistical, parametric, and systematic components,

$$\chi^2 = \chi_{\text{stat}}^2 + \chi_{\text{par}}^2 + \chi_{\text{sys}}^2. \quad (71)$$

Following [30], we define the statistical component χ_{stat}^2 in the limit of “infinite bins,”

$$\chi_{\text{stat}}^2 = \int_0^{9 \text{ MeV}} dE_{\text{vis}} \frac{d\chi_{\text{stat}}^2}{dE_{\text{vis}}} = \int_0^{9 \text{ MeV}} dE_{\text{vis}} \left(\frac{S^*(E_{\text{vis}}) - S(E_{\text{vis}})}{\sqrt{S^*(E_{\text{vis}})}} \right)^2, \quad (72)$$

We have verified that this limit is already realized numerically by using $\gtrsim 250$ energy bins, irrespective of linear or logarithmic binning in E_{vis} .

The parametric component χ_{par}^2 is a quadratic penalty for the priors on the four oscillation parameters $p_i = \bar{p}_i \pm \sigma_i$ in Sec. V A,

$$\chi_{\text{par}}^2 = \sum_{i=1}^4 \left(\frac{p_i - \bar{p}_i}{\sigma_i} \right)^2. \quad (73)$$

The continuous parameter α , which interpolates between normal hierarchy ($\alpha = +1$) and inverted hierarchy ($\alpha = -1$) is left free in the fit.

Finally, we assume three systematic normalization factors $f_j = 1$ with 1σ errors $\pm s_j$ ($j = R, U, \text{Th}$). The factor f_R multiplies all (medium-baseline and far) reactor spectra with an assumed error $s_R = 0.03$. The factors f_U and f_{Th} multiply the U and Th geoneutrino spectra, respectively, with tentative errors $s_{\text{Th}} = s_U = 0.2$. The systematic χ^2 component is then

$$\chi_{\text{sys}}^2 = \sum_{j=R,U,\text{Th}} \left(\frac{f_j - 1}{s_j} \right)^2. \quad (74)$$

In principle, one might include further relevant systematics via appropriate penalties (the “pull method” [58]). For instance, energy scale uncertainties and pulls have been introduced in terms of linear [28] or even polynomial [17] parameterizations. However, it is not obvious that these parameterizations can cover peculiar nonlinear profiles for the energy scale errors [47], which may mimic the effects of the “wrong hierarchy” in the worst cases [34]. In this context, the issue of systematic shape uncertainties is not really captured just by increasing the systematic “pulls,” but requires dedicated studies; very recent examples have been worked out in [36, 42]. In this work we prefer to keep χ_{sys}^2 as simple as in Eq. (74) and to separately discuss the subtle interplay of energy scale and spectrum shape uncertainties in Sec. VII.

The total χ^2 used hereafter is a function of eight parameters, including the f_j ’s,

$$\chi^2 = \chi^2(\delta m^2, \Delta m_{ee}^2, \theta_{12}, \theta_{13}, \alpha, f_R, f_U, f_{\text{Th}}). \quad (75)$$

Numerically, the minimization procedure and the identification of isolines of $\Delta\chi^2 = \chi^2 - \chi_{\text{min}}^2$ is performed through a Markov Chain MonteCarlo method [59]. By construction, minimization yields $\chi_{\text{min}}^2 = 0$ when the spectrum S equals the “true” one S^* . We shall typically show iso- N_σ contours, where $N_\sigma = \sqrt{\Delta\chi^2}$. Projections of such contours over a single parameter provide the bounds at N_σ standard deviations on such parameter [43]. It is understood that undisplayed parameters are marginalized away.

A final comment is in order. We surmise that, when real data will be available, the most powerful statistical analysis will involve maximization of unbinned (or finely binned) likelihood in both energy and time domain, as already performed in the context of KamLAND results [60, 61]. Such an analysis allows to include any kind of systematic errors via pulls, and helps to separate, on a statistical basis, stationary backgrounds (e.g., geoneutrinos) from time-evolving reactor fluxes, thus enhancing the statistical significance of the relevant signals [60, 61]. However, a refined time-energy analysis will probably be restricted only to the experimental collaboration owning the data, since the detailed reactor core evolution information is generally either classified or averaged over long (yearly or monthly) time periods.

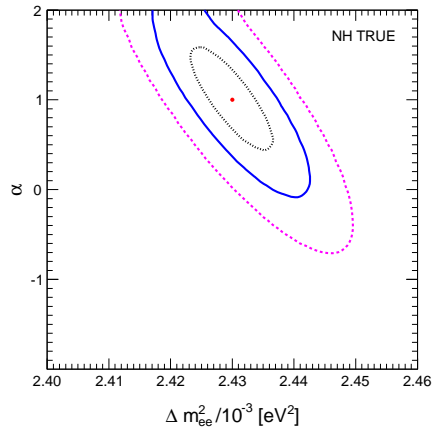


FIG. 7: Constraints in the plane $(\Delta m_{ee}^2, \alpha)$ at 1, 2 and 3σ ($\Delta\chi^2 = 1, 4, 9$) from a fit to prospective JUNO data assuming true normal hierarchy ($\alpha = +1$). Although the inverted hierarchy case ($\alpha = -1$) is $\sim 3.4\sigma$ away, the hierarchy discrimination is already compromised at $\sim 1.7\sigma$, where the “undecidable” case ($\alpha = 0$) is allowed.

VI. RESULTS OF THE ANALYSIS

We discuss below the results of our statistical analysis of prospective JUNO data as defined in the previous Section. We focus on the case of true NH, the results for true IH being rather symmetrical.

Figure 7 shows the results of the fit in the plane $(\Delta m_{ee}^2, \alpha)$ for true NH, in terms of $N_\sigma = 1, 2, 3$ contours for one parameter ($\Delta\chi^2 = 1, 4, 9$), all other parameters being marginalized away. The errors are rather linear on both parameters, and appear to be significantly anti-correlated. The anti-correlation stems from the tendency of the fit to keep constant the oscillation phase $2\Delta_{ee} + \alpha\varphi$ in Eq. (58) for typical neutrino energies $E \simeq 3\text{--}5$ MeV: an increase of Δm_{ee}^2 is then compensated by a decrease in α .

In Fig. 7, the case of wrong hierarchy ($\alpha = -1$) is formally reached at $\sim 3.4\sigma$; however, it would be misleading to take this “distance” as a measure of the sensitivity to the hierarchy. Physically, the discrimination of NH vs IH is successful if the data allow to tell the sign of a non- L/E phase, which advances or retards a hierarchy-independent L/E oscillation phase. In our adopted formalism, this requirement amounts to tell the sign of α : when the sign is undecidable ($\alpha \simeq 0$), the discrimination is already compromised. Therefore, the sensitivity to the hierarchy is more properly measured by the “distance” of the true case (either $\alpha = +1$ or $\alpha = -1$) from the null case ($\alpha = 0$): $N_\sigma \simeq \sqrt{\chi^2(\alpha = \pm 1) - \chi^2(\alpha = 0)}$. In Fig. 7, this distance is $\sim 1.7\sigma$, namely, about 1/2 of the ~ 3.4 sigma which formally separate the NH and IH cases. Thus, we recover independently the approximate “factor of two” reduction of the sensitivity with respect to naive expectations [30, 37, 38], as expressed by the “rule of thumb” $N_\sigma \simeq 0.5\sqrt{\Delta\chi^2(\text{NH} - \text{IH})}$ [42]. Our approach reaches such result via a fit to a continuous parameter (α), which is conveniently treated as any other floating parameters in the statistical analysis. The case of true IH (not shown) is very similar, with only a slight enhancement of the sensitivity to the hierarchy ($\sim 1.8\sigma$ instead of $\sim 1.7\sigma$).

In conclusion, the results in Fig 7 show that the sign of α (i.e., the advancement or retardation of phase due to the hierarchy) can be determined at a level slightly below $\sim 2\sigma$. This value is in the same ballpark of all recent estimates under similar assumptions, but has been derived via a different approach. In particular, we have recovered the “rule of thumb” $N_\sigma \simeq 0.5\sqrt{\Delta\chi^2(\text{NH} - \text{IH})}$ that was found and discussed in [30, 37, 38, 42] for two alternative discrete cases, by connecting the two cases via a continuous variable α , whose sign tells the hierarchy. The hierarchy discrimination is successful if the data prefer $|\alpha| = 1$ with sufficient significance with respect to $\alpha = 0$; conversely, a preference for $\alpha = 0$ would compromise the experiment, while surprisingly large values $|\alpha| \gg 1$ would signal possible systematics which are artificially enhancing the hierarchy effects. If the hierarchy discrimination is successful, then fit results such as those in Fig. 7 provide the central value and error of Δm_{ee}^2 and also of Δm^2 via Eq. (41), namely:

$$\Delta m^2 = \Delta m_{ee}^2 - \frac{\text{sign}(\alpha)}{2}(c_{12}^2 - s_{12}^2)\delta m^2. \quad (76)$$

The determination of the fundamental parameter Δm^2 thus depend also on the constraints achievable on the parameters $(\delta m^2, s_{12}^2)$, which we now discuss.

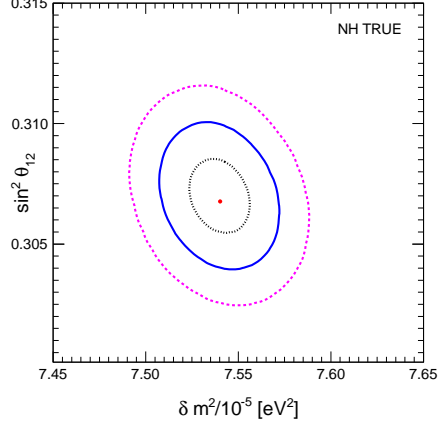


FIG. 8: Constraints in the plane $(\delta m^2, s_{12}^2)$ at 1, 2 and 3σ from a fit to prospective JUNO data, assuming true normal hierarchy.

Figure 8 shows the fit results in the plane $(\delta m^2, s_{12}^2)$ at 1, 2 and 3σ . The slight anti-correlation is due to the fact that, in general, a slight increase of the “slow” oscillation phase δ can be partly compensated by a decrease of the corresponding amplitude $\sin^2(2\theta_{12})$. The 1σ errors on each parameter correspond to a nominal accuracy of a few permill, i.e., one order of magnitude better than the current experimental constraints. Such a prospective accuracy makes it evident, a posteriori, the importance of including sub-percent effects due to propagation in matter (which affect both s_{12}^2 and δm^2 , see Sec. IV C) and to nucleon recoil (which affect δm^2 via the $\delta m^2/E$ dependence and the positron energy reconstruction, see Sec. III). Energy scale nonlinearities (see next Section) must also be kept under control at a similar level of accuracy, in order to avoid biased determinations of δm^2 .

Figure 9 shows the prospective constraints in the plane (f_R, s_{13}^2) . The two parameters are positively correlated, since an increase in the reactor flux normalization can be partly compensated by a higher s_{13}^2 enhancing electron flavor disappearance. In any case, the improvement on the s_{13}^2 accuracy is moderate: the prior $\sim 10\%$ error on this parameter becomes just $\sim 7\%$ after the fit.

Table I summarizes the information about the parameter accuracy in terms of fractional percent errors at 1σ , before and after the fit to prospective JUNO data, assuming either normal or inverted true hierarchy. In order to average out small nonlinearities and asymmetries, posterior fractional errors are defined as $1/6$ of the $\pm 3\sigma$ fit range, divided by the central value of the parameter (which, by construction, is the same before and after the fit). We also report the results without the far reactor or geoneutrino backgrounds, so as to gauge their impact on the final accuracy.

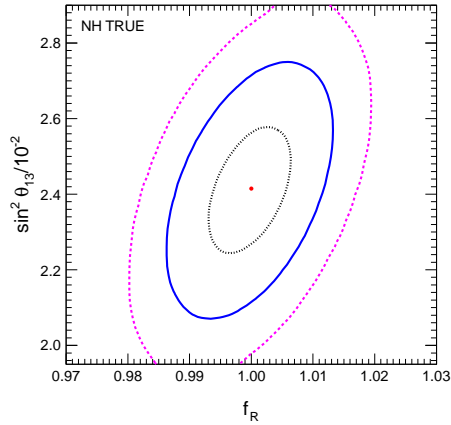


FIG. 9: Constraints in the plane (f_R, s_{13}^2) at 1, 2 and 3σ from a fit to prospective JUNO data assuming true normal hierarchy.

TABLE I: Statistical analysis of prospective JUNO data: fractional percent errors (1σ) on the free parameters, before and after the fit to prospective JUNO data, assuming either normal or inverted true hierarchy. The hypothetical cases without contributions from far reactors (“all – far”) or from geoneutrinos (“all – geo”) are also reported. In the latter case, the normalization factors $f_{\text{Th,U}}$ are absent.

Parameter	% error (prior)	% error after fit (NH true)			% after fit (IH true)		
		all data	all – far	all – geo	all data	all – far	all – geo
α	∞	59.2	59.0	57.0	56.2	55.3	54.0
Δm_{ee}^2	2.0	0.26	0.25	0.26	0.26	0.25	0.25
δm^2	3.2	0.22	0.21	0.16	0.21	0.21	0.16
s_{12}^2	5.5	0.49	0.47	0.39	0.49	0.46	0.42
s_{13}^2	10.3	6.95	6.88	6.95	6.84	6.77	6.84
f_R	3.0	0.66	0.66	0.64	0.65	0.65	0.64
f_{Th}	20.0	15.3	14.6	—	15.5	15.4	—
f_U	20.0	13.3	13.3	—	13.3	13.3	—

Table I shows that the cases of true NH and IH are almost equivalent in term of final accuracy on the fit parameters. In particular, α is determined to be $+1.00 \pm 0.59$ for true NH and -1 ± 0.56 for true IH. Concerning the other parameters, prospective JUNO data always lead to a reduction of the prior uncertainty, which is very significant for $(\Delta m_{ee}^2, \delta m^2, s_{12}^2, f_R)$ and moderate for the $(s_{13}^2, f_{\text{Th}}, f_U)$. The far-reactor background does not appear to affect significantly any fit parameter, while the geoneutrino background and its uncertainties tend to degrade somewhat the final accuracy of the mass-mixing parameters $(\delta m^2, s_{12}^2)$, whose observable oscillation cycle mainly falls in the geoneutrino energy region (see Fig. 5). Indeed, the $(\delta m^2, s_{12}^2)$ parameters have non negligible correlations with the geoneutrino normalization factors (f_{Th}, f_U) after the fit (not shown).

Finally, we discuss the contributions to the χ^2 difference between “true” and “wrong” hierarchy, assuming for definiteness the case of true NH as in Fig. 7. The best fit for fixed $\alpha = -1$ (wrong hierarchy) is reached at $\chi^2 = 11.7$, and is dominated by the statistical contribution ($\chi_{\text{stat}}^2 = 11.5$). Figure 10 shows the corresponding χ_{stat}^2 density, namely, the integrand of Eq. (72), as function of the visible energy E_{vis} , together with its cumulative distribution (i.e., the integral of the density with running upper limit). It can be seen that 80% of the contribution to the χ^2 comes from the spectral fit in a very small range at low energy, $E_{\text{vis}} \in [1.5, 3.5]$ MeV. In this range, the vertical mismatch between the true and wrong spectra changes sign many times, leading to a wavy pattern of the χ^2 density, also visible with smaller amplitude at higher energies. Intuitively, one can recognize that this wavy pattern is very fragile under small relative changes of the horizontal scale between the true and wrong spectra, due to possible energy scale uncertainties which, in the worst cases, might largely erase the pattern itself, at least at low energy. The next Section is devoted to a discussion of this issue, whose relevance was pointed out in [34].

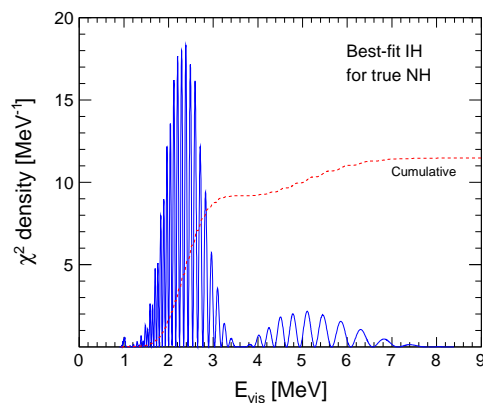


FIG. 10: Density and cumulative distribution functions for χ_{stat}^2 in the case of “wrong” inverted hierarchy, assuming “true” normal hierarchy. The cumulative function values can be read on the same vertical axis as for the density, but in dimensionless units.

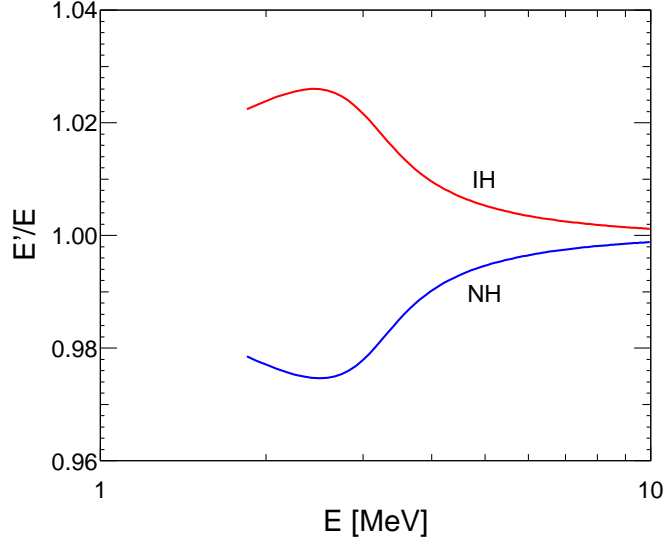


FIG. 11: Profile of the neutrino energy ratio E'/E which flips the sign of the hierarchy-dependent phase φ in the JUNO experiment, for the case $\Delta m_{ee}^2 = \Delta m_{ee}^{2'}$. The profiles for true NH and true IH are shown for $E \geq E_T = 1.806$ MeV.

VII. ENERGY SCALE AND SPECTRAL SHAPE UNCERTAINTIES

It was observed in [34] that changes in energy scale ($E \rightarrow E'$) at percent level can flip the sign of the hierarchy-dependent phase φ in Eq. (58) (namely, $\alpha = \pm 1 \rightarrow \alpha = \mp 1$), provided that

$$\frac{\Delta m_{ee}^2 L}{2E} \pm \varphi(E) = \frac{\Delta m_{ee}^{2'} L}{2E'} \mp \varphi(E'), \quad (77)$$

where $\Delta m_{ee}^2 \neq \Delta m_{ee}^{2'}$ in general. Multiplying the above terms by $2E'/L\Delta m_{ee}^2$ one gets an implicit equation for the ratio E'/E , which is amenable to iterative solutions by taking $\varphi(E)$ as in Eq. (45). The first iteration after the trivial solution ($E \simeq E'$) yields the compact expression:

$$\frac{E'}{E} \simeq \frac{\Delta m_{ee}^{2'}}{\Delta m_{ee}^2} \mp 2s_{12}^2 \frac{\delta m^2}{\Delta m_{ee}^2} \left(1 - \frac{\sin \delta(E)}{2\delta(E)\sqrt{P_{\text{vac}}^{2\nu}(E)}} \right), \quad (78)$$

which is already a very good approximation to the exact numerical solution of Eq. (77), as we have verified in a number of cases. Note that the upper (lower) sign refer to true NH (IH). Equation (78) usefully separates the linear and nonlinear terms which can jointly flip the sign of the phase φ in the transformation $E \rightarrow E'$.

It has been shown that transformations $E \rightarrow E'$ as in Eq. (78) can compromise the hierarchy determination [34, 36, 42], even if they do not lead to a complete degeneracy between the observable spectra in NH and IH. Below we discuss in detail two specific cases in the context of the JUNO project, and then we make some general comments.

A. Energy scale transformation $E \rightarrow E'$ with $E = E'$ at high energy

Let us specialize Eq. (78) by selecting the sub-case with $\Delta m_{ee}^2 = \Delta m_{ee}^{2'}$. In this case, the function E'/E takes the nonlinear form reported in Fig. 11, where the curves for true NH and IH tend to unit value at high energy (see also [34]). For definiteness, we consider the case of true NH, the case of true IH being qualitatively very similar. Several consequences emerge in the fit, which deserves a detailed discussion.

First of all, the parameter α is shifted from the true value $\alpha = +1$ to a wrong fitted value $\alpha \simeq -1$, as expected from the sign flip of φ . Figure 12 shows this shift in the plane $(\Delta m_{ee}^2, \alpha)$, to be compared with the results in Fig. 7. It appears the error ellipses are moved downwards from $\alpha = +1$ to $\alpha \simeq -1$ at nearly the same value of Δm_{ee}^2 .

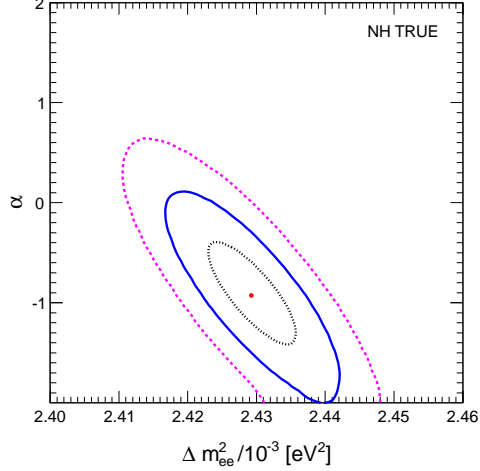


FIG. 12: Constraints in the plane $(\Delta m_{ee}^2, \alpha)$ for true NH, with energy scale variations as in Fig. 11. (Compare with Fig. 7.)

However, at the preferred point $(\Delta m_{ee}^2, \alpha) \simeq (2.43 \times 10^{-3} \text{ eV}^2, -1)$ in Fig. 12, the best fit is very poor, being characterized by $\chi^2 \simeq 360$. The reason is that, as also recently observed in [36, 42], the degeneracy induced by the transformation $E \rightarrow E'$ is never exact, since it also changes other spectral ingredients besides the oscillation phase φ . In particular, in our numerical experiment, it leads to a noticeable energy shift of $\simeq 2.2\%$ close to the energy threshold, as one can read directly from Fig. 11. As a result, the rapidly rising part of the spectrum just above threshold moves by the same amount, and the agreement between expected and observed spectra at low energy is compromised, as it can be seen in Fig. 13. The analysis of the χ^2 density in Fig 14 confirms that the energy scale shift $E \rightarrow E'$ does erase the wavy pattern in Fig. 10 (as a consequence of the sign flip of φ), but it also leads to a large increase of the χ^2 just around the threshold and, to a much lesser extent, around the two step-like features of the geoneutrino energy spectrum. Therefore, the low-energy part of the observed spectrum may act as a self-calibrating tool to diagnose energy scale shifts at percent level near the known IBD threshold ($E_T = 1.806 \text{ MeV}$).⁴

However, the possible self-calibration of the low-energy spectrum tail may fail, if the spectral shape itself is not

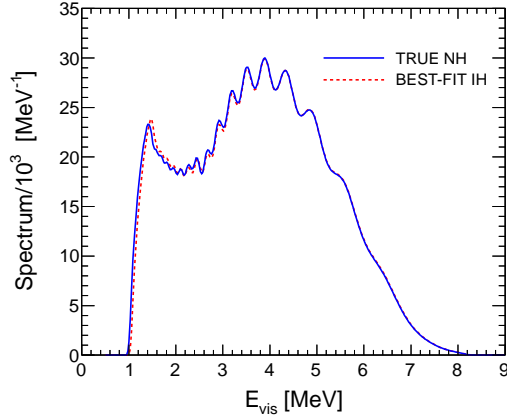


FIG. 13: Comparison of the true NH spectrum with the best-fit IH spectrum from Fig. 12.

⁴ Additional effects (not shown) induced by the energy scale transformation in Fig. 11 include shifts of best-fit parameters $(\delta m^2, s_{12}^2)$ and (f_U, f_{Th}) by $\sim 1\sigma$ – 2σ , in units of standard deviations after the fit (see Table I). Therefore, energy scale errors tend also to significantly bias such parameters, while the corresponding biases on the (f_R, s_{13}^2) parameters are found to be $< 1\sigma$ in our analysis.

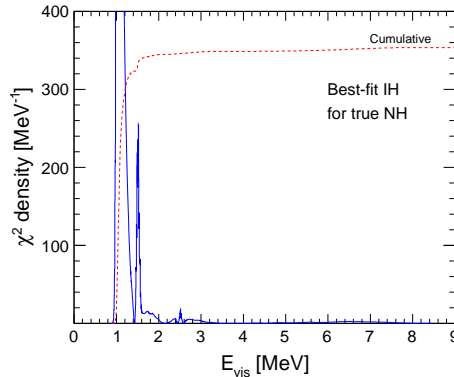


FIG. 14: χ^2 density and its cumulative distribution for the best-fit IH point in Fig. 12. At low energy, the density function reaches very high values which are partly out of scale.

accurately known in that region. In particular, if the shape errors in the observable reactor spectrum $\Phi\sigma$ (where Φ is the reactor flux and σ is the IBD cross section) are comparable to the deviations $\Phi(E)\sigma(E) \rightarrow \Phi(E')\sigma(E')$ induced by $E \rightarrow E'$, then most of the low-energy spectral changes can be “undone” by a fudge factor $f(E)$ with the following energy profile:

$$f(E) = \frac{\Phi(E)\sigma(E)}{\Phi(E')\sigma(E')}, \quad (79)$$

in which case the best-fit spectrum for the wrong hierarchy becomes almost completely indistinguishable from the original, true-hierarchy spectrum. In other words, the simultaneous occurrence of an energy scale transformation as in Eq. (78) and of a spectral deformation as in Eq. (79) make the true and wrong hierarchies nearly degenerate from a phenomenological viewpoint.

Figure 15 shows the fudge factor $f(E)$ corresponding to the specific transformation $E \rightarrow E'$ with $\Delta m_{ee}^2 = \Delta m_{ee'}^2$, for both NH and IH. The factor diverges at threshold but, for neutrino energies sufficiently above E_T (say, $E \gtrsim 2.1$ MeV) it takes values of $O(10\%)$, and can become as low as $O(2\%)$ in the high-energy part of the spectrum. Shape variations of about this size may still be tolerated within current uncertainties on the reactor spectrum [56, 62], and thus should be kept under control in future JUNO-like experiments.

If one applies, at the same time, the transformation $E \rightarrow E'$ in Fig. 11 and the fudge factor $f(E)$ in Fig. 15 to the case of true NH, the results in Fig. 12 remain basically the same (i.e., the “wrong” IH is preferred), but the spectral mismatch around threshold in Fig. 13 is largely cured, and the total χ^2 in Fig. 14 drops from ~ 360 to ~ 22 . In this case, the best-fit IH spectrum is almost completely degenerate with the true NH spectrum.

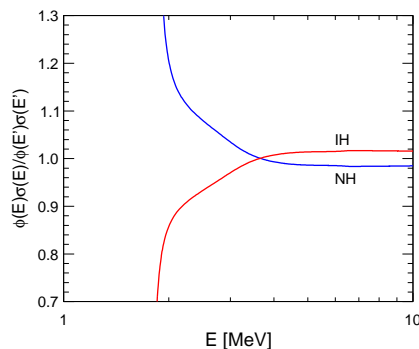


FIG. 15: Energy profiles of the fudge factors which would “undo” the reactor spectral changes induced by the changes $E \rightarrow E'$ reported in Fig. 11.

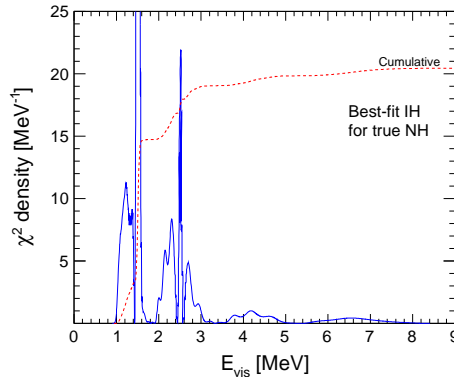


FIG. 16: χ^2 density and its cumulative distribution at best fit, after modifying the shape of the reactor energy spectrum as in Fig. 15. To be compared with Fig. 14; see the text for details.

Fig. 16 shows the corresponding χ^2 density, which is now dominated by the residual shape mismatch of the geoneutrino energy spectrum, whose step-like features still occur “at the wrong energy” and slightly break the degeneracy. Geoneutrinos thus offer an additional handle to self-calibrate the low-energy scale to some extent, as also pointed out in another context [63].

Summarizing, an energy scale transformation as in Fig. 11 is able to swap the hierarchy in the fit (Fig. 12), but it also induces a mismatch in the spectral features around threshold (Fig. 13) and thus a very high χ^2 value at best fit (Fig. 14), which could be used as a diagnostic, self-calibration tool. However, specific variations of the reactor spectrum shape (Fig. 15) can largely “undo” the low-energy mismatch, leaving only a residual misfit in the geoneutrino spectral shapes (Fig. 16) which could be used a secondary self-calibration tool. There is thus a subtle interplay between energy scale systematics and spectral shape uncertainties, which need to be kept under control in order to discriminate the hierarchy and to get unbiased estimates of the ν_e oscillation parameters.

B. Energy scale transformation $E \rightarrow E'$ with $E = E'$ at threshold

In the previous section, it has been shown that the specific choice $\Delta m_{ee}^2 = \Delta m_{ee}^{\prime 2}$ in Eq. (78) leads to both energy scale and spectral variations mainly localized at relatively low energies, $E_{\text{vis}} \lesssim 3$ MeV. However, other choices in Eq. (78) may move the relevant variations to the high-energy part of the spectrum. In particular, one may choose the ratio $\Delta m_{ee}^{\prime 2}/\Delta m_{ee}^2$ in Eq. (78) so as to get $E/E' = 1$ just at threshold ($E = E_T$). For the considered JUNO set up, this choice corresponds to take $\Delta m_{ee}^{\prime 2}/\Delta m_{ee}^2 \simeq 1.022$ (0.978) for true NH (IH). Figure 17 shows the corresponding profile of the energy ratio E/E' , which is $\lesssim 2$ permil for $E \lesssim 3$ MeV, but grows up to $\sim 2\%$ at higher energies.

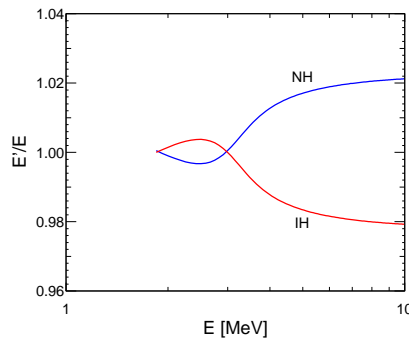


FIG. 17: Profile of the neutrino energy ratio E'/E which flips the sign of the hierarchy-dependent phase φ in the JUNO experiment, for the case $\Delta m_{ee}^{\prime 2}/\Delta m_{ee}^2 \simeq 1.022$ (0.978) in NH (IH). The profiles are shown for $E \geq E_T = 1.806$ MeV.

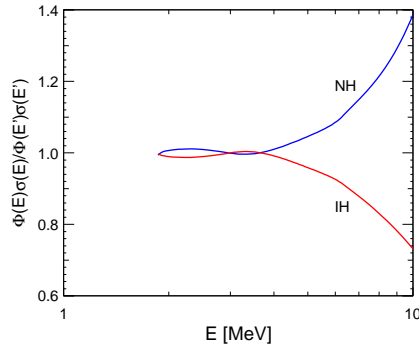


FIG. 18: Energy profiles of the fudge factors which would “undo” the reactor spectral changes induced by the changes $E \rightarrow E'$ reported in Fig. 17.

If we fit the prospective JUNO data (for true NH) with $E \rightarrow E'$ as in Fig. 17, the preferred value of α is shifted down to ~ -1 (similarly to Fig. 12), and the best-fit value of $\Delta m_{ee}^2/(10^{-3} \text{ eV}^2)$ is shifted to $\sim 2.48 \simeq 1.022 \times 2.43$ as expected (not shown). In this case, the effect of the energy scale variation in Fig. 17 is quite dramatic: at best fit, not only the wrong hierarchy is preferred, but the value of Δm_{ee}^2 is biased by an order of magnitude more than its prospective 1σ accuracy (as reported in Table I). However, also in this case the degeneracy between the spectra for true and wrong hierarchy is not complete: the best fit in the “wrong” IH is very bad ($\chi^2 \simeq 280$), and receives contributions mainly from the high-energy part of the spectrum, $E_{\text{vis}} \gtrsim 3 \text{ MeV}$ (not shown).

A misfit of the high-energy tail of the spectrum might be used as a diagnostic of systematic energy scale deviations in that region; however, the misfit could be largely compensated by appropriate variations of the reactor spectrum shape via a fudge factor $f(E)$, analogously to the case discussed in the previous section. Figure 18 shows the fudge factor which brings the best-fit spectrum for the wrong hierarchy in much closer agreement with the original spectrum for the true hierarchy (either normal or inverted), for energy variations as in Fig. 17. If deviations as large as in Fig. 18 are allowed within reactor spectral shape uncertainties [56, 62], then the degeneracy between true and wrong hierarchy would be almost complete along the whole energy range, with residual misfits located mainly in the geoneutrino energy region. Indeed, by applying the fudge factor in Fig. 18, the “wrong” hierarchy is still preferred, but the χ^2 at best fit drops by an order of magnitude, and the best-fit value of Δm_{ee}^2 is brought back to the original value $\sim 2.43 \times 10^{-3} \text{ eV}^2$ (not shown).

C. Further comments on energy scale and spectral shape deviations

The simultaneous occurrence of energy scale deviations $E \rightarrow E'$ as in Eq. (78) and of reactor spectral shape deviations $f(E)$ as in Eq. (79) makes true and wrong hierarchies nearly degenerate across the whole visible energy range, with small residual misfits mainly located in the geoneutrino energy region. If such deviations are allowed within the systematic uncertainties of the JUNO experiment, the discrimination of the hierarchy would be seriously compromised, being degraded at significance level necessarily lower than the $\sim 2\sigma$ estimated in Sec. VI.

At present it is premature—if not impossible—to guess the final accuracy on the energy scale achievable with dedicated calibration experiment and detector simulations, as well as the reduction of spectral shape uncertainties reachable after the current campaign of high-statistics, near-detector measurements. It is also not particularly useful to embed such deviations by means of arbitrary functional forms (e.g., polynomials) and corresponding pulls in the fit, unless such functions can also cover the family of nonlinear deviations implied by Eqs. (78) and (79) [see also [36, 42]]. We are thus approaching a new and unusual situation in neutrino physics, which was already highlighted in another context [64]: spectral measurements with very high statistics require dedicated studies of the “shape” of nonlinear systematics, which are not necessarily captured by simply adding a few more pulls and penalties in the fit.

Finally, we emphasize that, in our approach with free α , the discrimination of the hierarchy is already compromised when $\alpha = \pm 1$ is misfitted as $\alpha = 0$ (case of “undecidable” hierarchy) rather than as $\alpha = \mp 1$ (case of “wrong” hierarchy). In particular, the energy scale deviation which would bring $\alpha = \pm 1$ to $\alpha = 0$ (“canceling” the hierarchy-dependent oscillation phase φ) obeys the equation:

$$\frac{\Delta m_{ee}^2 L}{2E} \pm \varphi(E) = \frac{\Delta m_{ee}^{2'} L}{2E'}, \quad (80)$$

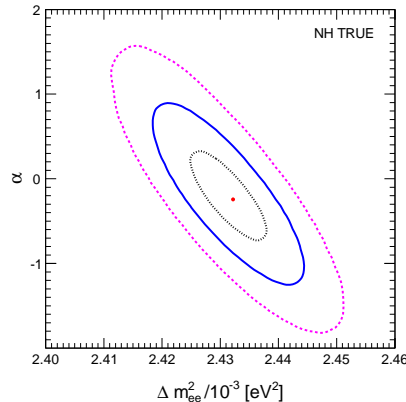


FIG. 19: Constraints in the plane $(\Delta m_{ee}^2, \alpha)$ for true NH, after applying the energy scale variations of Fig. 11 reduced by a factor of two. The best fit is roughly half-way between the true hierarchy ($\alpha = +1$) and the wrong hierarchy ($\alpha = -1$). See the text for details.

which is approximately solved by

$$\frac{E'}{E} \simeq \frac{\Delta m_{ee}^{2'}}{\Delta m_{ee}^2} \mp s_{12}^2 \frac{\delta m^2}{\Delta m_{ee}^2} \left(1 - \frac{\sin \delta(E)}{2\delta(E)\sqrt{P_{\text{vac}}^{2\nu}(E)}} \right). \quad (81)$$

In comparison with Eq. (78), the nonlinear term in the above equation is a factor of two smaller. Therefore, energy scale deviations of about half the size discussed in the previous two Sections (as well as spectral deviations $f(E)$ reduced by a similar factor) are already sufficient to compromise the hierarchy determination, bringing the fit close to the null case $\alpha = 0$, as we have explicitly verified numerically in various cases. For instance, Fig. 19 shows the fit results assuming $\Delta m_{ee}^{2'} = \Delta m_{ee}^2$ in Eq. (81). In this case, the deviations of E'/E from unity are exactly 1/2 smaller than in Fig. 11, and the true value $\alpha = 1$ is misfitted as $\alpha \simeq -0.2 \pm 0.5$ at $\pm 1\sigma$, which is more consistent with $\alpha = 0$ (undecidable hierarchy) than with $\alpha = \pm 1$ (true or wrong hierarchy). In this respect, it is useful to compare Fig. 19 with both Fig. 7 (best fit at the true hierarchy) and Fig. 12 (best fit at the wrong hierarchy).

In a sense, the challenge of the energy scale may actually be greater than pointed out in [34] and [36, 42]), by approximately a factor of two. In particular, in order to reject cases leading to $\alpha \simeq 0$ with, say, 3σ confidence, the ratio E'/E should be kept close to unity at the few permill level over the whole reactor neutrino energy range. Moreover, as shown in this section, the conspiracy of energy scale and spectrum shape systematics may lead to an even stronger degeneracy between cases with different values of α (e.g., $\alpha = \pm 1$ versus $\alpha = \mp 1$, or versus $\alpha = 0$), making it very difficult to prove the occurrence of a non- L/E oscillation phase φ with a definite sign. An additional detector close to the main reactors might help to mitigate the impact of such systematics (see [36, 42]), provided that the near and far detector responses are proven to be very similar at all energies, so as to cancel out correlated uncertainties on both the x and y axes of event spectra. All these delicate issues definitely require further investigations, in order to prove the feasibility of hierarchy discrimination at reactors with sufficient statistical significance.

VIII. SUMMARY AND CONCLUSIONS

Medium-baseline reactor neutrino experiments can offer unprecedented opportunities to probe, at the same time, all the parameters which govern the mixing of $\bar{\nu}_e$ with the neutrino mass states, namely, the mixing angles θ_{12} and θ_{13} , the two squared mass differences δm^2 and Δm^2 , and the hierarchy parameter α (+1 for NH and -1 for IH). These goals largely justify the current efforts towards the construction of such experiments, as currently envisaged by the JUNO and RENO-50 projects.

In this context, we have revisited some issues raised by the need of precision calculations and refined statistical analyses of reactor event spectra. In particular, we have shown how to include analytically IBD recoil effects in binned and unbinned spectra, via appropriate modifications of the energy resolution function (Sec. III). We have also generalized the oscillation probability formula by including analytically matter propagation and multiple reactor damping effects, and by treating the parameter α as a continuous — rather than discrete — variable (Sec. IV).

The determination of the hierarchy is then transformed from a test of hypothesis to a parameter estimation, with a sensitivity given by the statistical distance of the true case (either $\alpha = +1$ or $\alpha = -1$) from the “undecidable” case ($\alpha = 0$). Numerical experiments have been performed for the specific experimental set up envisaged for the JUNO experiment, assuming a realistic sample of $O(10^5)$ medium-baseline reactor events, plus geoneutrino and far-reactor backgrounds, via an unbinned χ^2 analysis. We have found a typical sensitivity to the hierarchy slightly below 2σ in JUNO, and significant prospective improvement upon current errors on the oscillation parameters (see Table I and Figs. 7–9), as far as systematic uncertainties are limited to reactor and geoneutrino normalization errors (Sec. V).

Further systematic uncertainties, associated to energy scale and spectrum shape distortions, may seriously compromise the hierarchy sensitivity and may also bias the oscillation parameters (Sec. VI). In particular, specific energy scale variations — for which we have provided compact expressions — can move the reconstructed value of α away from the true one; e.g., $\alpha = +1$ can be misfitted as $\alpha \simeq -1$ or as $\alpha \simeq 0$. However, the overall fit is generally very bad in such cases, since the reactor spectrum is also distorted at either low or high energies with respect to expectations. In principle, these shape distortions might be used as a diagnostic of energy scale errors; however, they might also be compensated by opposite ones within current shape uncertainties, in which case the degeneracy between “true” and “wrong” values of α would be almost complete (up to residual, unbalanced distortions of geoneutrino spectra). For instance, the joint occurrence of distortions as in Figs. 11 and 15 (or as in Figs. 17 and 18) would essentially flip the hierarchy parameter ($\alpha = \pm 1 \rightarrow \alpha \simeq \mp 1$) with only a modest increase in the χ^2 . Distortions of about half this size are sufficient to bring the fit close to the case of “undecidable hierarchy” as in Fig. 19 ($\alpha = \pm 1 \rightarrow \alpha \simeq 0$), thus compromising the hierarchy discrimination. It is thus very important to control, at the same time, the systematic uncertainties on both the x -axis (energy scale) and the y -axis (spectrum shape) of measured and simulated reactor event spectra, with an accuracy sufficient to reject the above distortions at high confidence level.

Acknowledgments

Acknowledgments. This work is supported by the Italian Istituto Nazionale di Fisica Nucleare (INFN) through the “Theoretical Astroparticle Physics” project.

-
- [1] G. L. Fogli, E. Lisi and A. Palazzo, “Quasi energy independent solar neutrino transitions,” *Phys. Rev. D* **65**, 073019 (2002) [hep-ph/0105080].
 - [2] S. T. Petcov and M. Piai, “The LMA MSW solution of the solar neutrino problem, inverted neutrino mass hierarchy and reactor neutrino experiments,” *Phys. Lett. B* **533**, 94 (2002) [hep-ph/0112074].
 - [3] See, e.g., the contributions at the recent dedicated International Workshop “RENO-50: Toward Neutrino Mass Hierarchy (Seoul, Korea, 13-14 June 2013). Website: home.kias.re.kr/MKG/h/reno50/
 - [4] S. Choubey, S. T. Petcov and M. Piai, “Precision neutrino oscillation physics with an intermediate baseline reactor neutrino experiment,” *Phys. Rev. D* **68**, 113006 (2003) [hep-ph/0306017].
 - [5] F. P. An *et al.* [Daya Bay Collaboration], “Observation of electron-antineutrino disappearance at Daya Bay,” *Phys. Rev. Lett.* **108**, 171803 (2012) [arXiv:1203.1669 [hep-ex]].
 - [6] F. P. An *et al.* [Daya Bay Collaboration], “Improved Measurement of Electron Antineutrino Disappearance at Daya Bay,” *Chin. Phys. C* **37**, 011001 (2013) [arXiv:1210.6327 [hep-ex]].
 - [7] J. K. Ahn *et al.* [RENO Collaboration], “Observation of Reactor Electron Antineutrino Disappearance in the RENO Experiment,” *Phys. Rev. Lett.* **108**, 191802 (2012) [arXiv:1204.0626 [hep-ex]].
 - [8] J. Jang for the RENO Collaboration, talk at the “RENO-50” Workshop [3].
 - [9] Y. Abe *et al.* [DOUBLE-CHOOZ Collaboration], “Indication for the disappearance of reactor electron antineutrinos in the Double Chooz experiment,” *Phys. Rev. Lett.* **108**, 131801 (2012) [arXiv:1112.6353 [hep-ex]].
 - [10] Y. Abe *et al.* [Double Chooz Collaboration], “Reactor electron antineutrino disappearance in the Double Chooz experiment,” *Phys. Rev. D* **86**, 052008 (2012) [arXiv:1207.6632 [hep-ex]].
 - [11] K. Abe *et al.* [T2K Collaboration], “Evidence of Electron Neutrino Appearance in a Muon Neutrino Beam,” arXiv:1304.0841 [hep-ex].
 - [12] M. Wilking for the T2K Collaboration, talk at EPS-HEP 2013, the European Physical Society Conference on High Energy Physics (Stockholm, Sweden, 2013), <http://eps-hep2013.eu>.
 - [13] P. Adamson *et al.* [MINOS Collaboration], “Electron neutrino and antineutrino appearance in the full MINOS data sample,” *Phys. Rev. Lett.* [arXiv:1301.4581 [hep-ex]].
 - [14] G. L. Fogli, E. Lisi, A. Marrone, A. Palazzo and A. M. Rotunno, “Evidence of $\theta_{13} > 0$ from global neutrino data analysis,” *Phys. Rev. D* **84**, 053007 (2011) [arXiv:1106.6028 [hep-ph]].
 - [15] G. L. Fogli, E. Lisi, A. Marrone, D. Montanino, A. Palazzo and A. M. Rotunno, “Global analysis of neutrino masses, mixings and phases: entering the era of leptonic CP violation searches,” *Phys. Rev. D* **86**, 013012 (2012) [arXiv:1205.5254 [hep-ph]].

- [16] J. Jang for the RENO Collaboration, talk at the “RENO-50” Workshop [3].
- [17] Y. -F. Li, J. Cao, Y. Wang and L. Zhan, “Unambiguous Determination of the Neutrino Mass Hierarchy Using Reactor Neutrinos,” arXiv:1303.6733 [hep-ex].
- [18] L. Zhan for the Daya Bay Collaboration, talk at the “RENO-50” Workshop [3].
- [19] Y. Wang, talk at the 2013 Lepton Photon Conference (San Francisco, CA, 2013), <http://www-conf.slac.stanford.edu/lp13>; talk at the 2013 EPS-HEP Conference (Stockholm, Sweden, 2013), <http://eps-hep2013.eu>
- [20] S. Schonert, T. Lasserre and L. Oberauer, “The HLMA project: Determination of high Δm^2 LMA mixing parameters and constraint on $|U_{e3}|$ with a new reactor neutrino experiment,” *Astropart. Phys.* **18**, 565 (2003) [hep-ex/0203013].
- [21] A. de Gouvea, J. Jenkins and B. Kayser, “Neutrino mass hierarchy, vacuum oscillations, and vanishing $-U(e3)-$,” *Phys. Rev. D* **71**, 113009 (2005) [hep-ph/0503079].
- [22] H. Nunokawa, S. J. Parke and R. Zukanovich Funchal, “Another possible way to determine the neutrino mass hierarchy,” *Phys. Rev. D* **72**, 013009 (2005) [hep-ph/0503283].
- [23] H. Minakata, H. Nunokawa, S. J. Parke and R. Zukanovich Funchal, “Determination of the neutrino mass hierarchy via the phase of the disappearance oscillation probability with a monochromatic anti-electron-neutrino source,” *Phys. Rev. D* **76**, 053004 (2007) [Erratum-ibid. *D* **76**, 079901 (2007)] [hep-ph/0701151].
- [24] J. Learned, S. T. Dye, S. Pakvasa and R. C. Svoboda, “Determination of neutrino mass hierarchy and θ_{13} with a remote detector of reactor antineutrinos,” *Phys. Rev. D* **78**, 071302 (2008) [hep-ex/0612022].
- [25] L. Zhan, Y. Wang, J. Cao and L. Wen, “Determination of the Neutrino Mass Hierarchy at an Intermediate Baseline,” *Phys. Rev. D* **78**, 111103 (2008) [arXiv:0807.3203 [hep-ex]].
- [26] L. Zhan, Y. Wang, J. Cao and L. Wen, “Experimental Requirements to Determine the Neutrino Mass Hierarchy Using Reactor Neutrinos,” *Phys. Rev. D* **79**, 073007 (2009) [arXiv:0901.2976 [hep-ex]].
- [27] M. Batygov, S. Dye, J. Learned, S. Matsuno, S. Pakvasa and G. Varner, “Prospects of neutrino oscillation measurements in the detection of reactor antineutrinos with a medium-baseline experiment,” arXiv:0810.2580 [hep-ph].
- [28] P. Ghoshal and S. T. Petcov, “Neutrino Mass Hierarchy Determination Using Reactor Antineutrinos,” *JHEP* **1103**, 058 (2011) [arXiv:1011.1646 [hep-ph]].
- [29] P. Ghoshal and S. T. Petcov, “Addendum: Neutrino Mass Hierarchy Determination Using Reactor Antineutrinos,” *JHEP* **1209**, 115 (2012) [arXiv:1208.6473 [hep-ph]].
- [30] S. -F. Ge, K. Hagiwara, N. Okamura and Y. Takaesu, “Determination of mass hierarchy with medium baseline reactor neutrino experiments,” *JHEP* **1305**, 131 (2013) [arXiv:1210.8141 [hep-ph]].
- [31] E. Ciuffoli, J. Evslin and X. Zhang, “The Neutrino Mass Hierarchy at Reactor Experiments now that θ_{13} is Large,” *JHEP* **1303**, 016 (2013) [arXiv:1208.1991 [hep-ex]].
- [32] E. Ciuffoli, J. Evslin and X. Zhang, “The Neutrino Mass Hierarchy from Nuclear Reactor Experiments,” arXiv:1302.0624 [hep-ph].
- [33] E. Ciuffoli, J. Evslin and X. Zhang, “Mass Hierarchy Determination Using Neutrinos from Multiple Reactors,” *JHEP* **1212**, 004 (2012) [arXiv:1209.2227 [hep-ph]].
- [34] X. Qian, D. A. Dwyer, R. D. McKeown, P. Vogel, W. Wang and C. Zhang, “Mass Hierarchy Resolution in Reactor Anti-neutrino Experiments: Parameter Degeneracies and Detector Energy Response,” *PRD*, **87**, **033005** (2013) [arXiv:1208.1551 [physics.ins-det]].
- [35] E. Ciuffoli, J. Evslin, Z. Wang, C. Yang, X. Zhang and W. Zhong, “Medium Baseline Reactor Neutrino Experiments with 2 Identical Detectors,” arXiv:1211.6818 [hep-ph].
- [36] E. Ciuffoli, J. Evslin, Z. Wang, C. Yang, X. Zhang and W. Zhong, “Advantages of Multiple Detectors for the Neutrino Mass Hierarchy Determination at Reactor Experiments,” arXiv:1308.0591 [hep-ph].
- [37] X. Qian, A. Tan, W. Wang, J. J. Ling, R. D. McKeown and C. Zhang, “Statistical Evaluation of Experimental Determinations of Neutrino Mass Hierarchy,” *Phys. Rev. D* **86**, 113011 (2012) [arXiv:1210.3651 [hep-ph]].
- [38] E. Ciuffoli, J. Evslin and X. Zhang, “Confidence in a Neutrino Mass Hierarchy Determination,” arXiv:1305.5150 [hep-ph].
- [39] H. Minakata, “Phenomenology of future neutrino experiments with large $\Theta(13)$,” *Nucl. Phys. Proc. Suppl.* **235-236**, 173 (2013) Proceedings of *Neutrino 2012*, XXV International Conference on Neutrino Physics and Astrophysics (Kyoto, Japan, 2012), ed. by T. Kobayashi, M. Nakahata and T. Nakaya [arXiv:1209.1690 [hep-ph]].
- [40] W. Winter, “Neutrino mass hierarchy determination with IceCube-PINGU,” arXiv:1305.5539 [hep-ph].
- [41] M. Blennow and T. Schwetz, “Determination of the neutrino mass ordering by combining PINGU and Daya Bay II,” arXiv:1306.3988 [hep-ph].
- [42] S. Kettell *et al.*, “Neutrino mass hierarchy determination and other physics potential of medium-baseline reactor neutrino oscillation experiments,” arXiv:1307.7419 [hep-ex], submitted to the Proceedings of the Community Summer Study *Snowmass 2013*, <http://www.snowmass2013.org>.
- [43] J. Beringer *et al.* (Particle Data Group), *Phys. Rev. D* **86**, 010001 (2012).
- [44] P. Vogel, “Analysis Of The Anti-neutrino Capture On Protons,” *Phys. Rev. D* **29**, 1918 (1984).
- [45] P. Vogel and J. F. Beacom, “Angular distribution of neutron inverse beta decay, $\bar{\nu}_e + p \rightarrow e^+ + n$,” *Phys. Rev. D* **60**, 053003 (1999) [hep-ph/9903554].
- [46] A. Strumia and F. Vissani, “Precise quasielastic neutrino/nucleon cross-section,” *Phys. Lett. B* **564**, 42 (2003) [astro-ph/0302055].
- [47] T. Classe, “A precise determination of the KamLAND energy scale,” Ph.D. Thesis (U. of Alabama, 2007).
- [48] I.S. Gradshteyn and I.M. Ryzhik, “Table of Integrals, Series, and Products”, ed. by A. Jeffrey and D. Zwillinger (Academic Press, San Diego, CA, 2007), 7th edition, 1171 pp.
- [49] B. Faid, G. L. Fogli, E. Lisi and D. Montanino, “Vacuum oscillations and variations of solar neutrino rates in Super-

- Kamiokande and Borexino,” *Astropart. Phys.* **10**, 93 (1999) [hep-ph/9805293].
- [50] J. LoSecco, “Optimization for Mass Hierarchy,” arXiv:1306.0845 [hep-ph].
- [51] X. Qian, A. Tan, W. Wang, J. J. Ling, R. D. McKeown and C. Zhang, “Statistical Evaluation of Experimental Determinations of Neutrino Mass Hierarchy,” *Phys. Rev. D* **86**, 113011 (2012) [arXiv:1210.3651 [hep-ph]].
- [52] E. Ciuffoli, J. Evslin and X. Zhang, “Confidence in a Neutrino Mass Hierarchy Determination,” arXiv:1305.5150 [hep-ph].
- [53] G. Fiorentini, G. L. Fogli, E. Lisi, F. Mantovani and A. M. Rotunno, “Mantle geoneutrinos in KamLAND and Borexino,” *Phys. Rev. D* **86**, 033004 (2012) [arXiv:1204.1923 [hep-ph]].
- [54] Y. Huang, V. Chubakov, F. Mantovani, R.L. Rudnick, and W.F. McDonough, “A reference Earth model for the heat producing elements and associated geoneutrino flux” [arXiv:1301.0365 [physics.geo-ph]].
- [55] M. Blennow and A. Y. Smirnov, “Neutrino propagation in matter,” *Adv. High Energy Phys.* **2013**, 972485 (2013) [arXiv:1306.2903 [hep-ph]].
- [56] P. Huber, “On the determination of anti-neutrino spectra from nuclear reactors,” *Phys. Rev. C* **84**, 024617 (2011) [Erratum-ibid. *C* **85**, 029901 (2012)] [arXiv:1106.0687 [hep-ph]].
- [57] G. Fiorentini, M. Lissia and F. Mantovani, “Geo-neutrinos and Earth’s interior,” *Phys. Rept.* **453**, 117 (2007) [arXiv:0707.3203 [physics.geo-ph]].
- [58] G. L. Fogli, E. Lisi, A. Marrone, D. Montanino and A. Palazzo, “Getting the most from the statistical analysis of solar neutrino oscillations,” *Phys. Rev. D* **66**, 053010 (2002) [hep-ph/0206162].
- [59] In order to produce and analyze the likelihood chains, we use a modified version of the CosmoMC (Cosmological Monte Carlo) from: A. Lewis and S. Bridle, *Phys. Rev. D* **66**, 103511 (2002).
- [60] G. L. Fogli, E. Lisi, A. Palazzo and A. M. Rotunno, “KamLAND neutrino spectra in energy and time: Indications for reactor power variations and constraints on the georeactor,” *Phys. Lett. B* **623**, 80 (2005) [hep-ph/0505081].
- [61] A. Gando *et al.* [KamLAND Collaboration], “Reactor On-Off Antineutrino Measurement with KamLAND,” arXiv:1303.4667 [hep-ex].
- [62] M. Fallot, S. Cormon, M. Estienne, A. Algora, V. M. Bui, A. Cucoanes, M. Elnimr and L. Giot *et al.*, “New antineutrino energy spectra predictions from the summation of beta decay branches of the fission products,” *Phys. Rev. Lett.* **109**, 202504 (2012) [arXiv:1208.3877 [nucl-ex]].
- [63] J. Kopp, M. Lindner and A. Merle, “Self-Calibration of Neutrino Detectors using characteristic Backgrounds,” *Nucl. Instrum. Meth. A* **582**, 456 (2007) [hep-ph/0703055].
- [64] E. Lisi, in the Proceedings of the International Workshop on “Sub-dominant oscillation effects in atmospheric neutrino experiments” (Kashiwa, Japan, 2004), *Frontier Science Series* **45** (Universal Academy Press, Tokyo, Japan, 2005), p. 19. Available at www-rccn.icrr.u-tokyo.ac.jp/rccnws04/